UNIVERSITAT POLITÈCNICA DE VALÈNCIA

ESCUELA TÉCNICA SUPERIOR INGENIERÍA INDUSTRIAL VALENCIA

TRABAJO FIN DE GRADO EN INGENIERÍA BIOMÉDICA

COMPUTATIONAL MODELLING AND SIMULATION OF THE MOUSE ATRIOVENTRICULAR NODE ACTION POTENTIAL

AUTHOR: Clara Sales Bellés

SUPERVISOR: Stefano Severi

SUPERVISOR: Chiara Bartolucci

Academic year: 2019-20

ABSTRACT

The purpose of this work is the computational modelling and simulation of the mouse atrioventricular node action potential. This project starts from an already existing computational model of this cell which needs to be improved by the introduction of calcium handling which will encourage a better representation of what is really happening in the cell considered.

These improvements consist in introducing the sarcoplasmic reticulum and calcium cycle and considering the intracellular ionic concentration as states variables which were taken into account as constants in the previous model. Its modelling will be based on a sinoatrial node model, developed by Matteo Mangoni in Jsim programming based on Kharche's model, and then it will be adjusted it to atrioventricular node characteristics. Moreover, some current reformulations based on Voltage-Clamp fitting from AVN experimental data is included in the presented model.

Therefore, the aim of the project is to develop an improved computational model of the atrioventricular node action potential by adding the components previously mentioned and presented as a first version model.

INDEX

LIST OF FIGURES

LIST OF TABLES

CHAPTER 1: MOTIVATION AND JUSTIFICATION

1.1 IMPORTANCE OF COMPUTATIONAL CARDIOLOGY MODELLING

Nowadays, it is not possible to understand medicine without the technological advance science has experimented through these last years. Mathematical modelling has been one of these improvements and it has become an important tool supporting decision-making in different healthcare scenarios. Moreover, the importance of being able to computationally reproduce physiological events resides in the capacity of simulation and prediction of any variable of interest modelled.

Computational cardiology is one of the different fields where mathematical modelling can be used in health. It allows a better understanding of what is happening in our heart from a nanoscale point of view to a macroscale one. Therefore, its utility is found in its power in helping both diagnosis and treatment of heart diseases.

1.2 IMPORTANCE OF COMPUTATIONAL CARDIOLOGY MODELLING FOCUSED ON AVN

This work is based on the simulation of the action potential (AP) of a single cell in the atrioventricular node (AVN). This node has not been widely studied from the computational cardiology point of view. Nevertheless, its function in the heart is crucial to control heart beating as it acts as a filter between atriums and ventricles and it is the secondary pacemaker.

The purpose of this work is to obtain a consistent and complete computational model of an action potential of an AVN single cell from an existent one where calcium handling was missing. The introduction of calcium handling is fundamental to reproduce a full representation of an action potential AVN cell due to the role that calcium has related to contraction. This implementation will lead this model to a second generation one due to the consideration of the cytosol compartmentalization and dynamics intracellular concentrations.

CHAPTER 2: INTRODUCTION

2.1 HEART'S BASIC KNOWLEDGE

The heart could be seen as the most important organ in our body as it is responsible for blood's circulation. Its function lies in bombing blood to every single part of the body, providing essential nutrients for each cell and eliminating the wastes which are made.

This section aims to introduce the heart's anatomy and physiology in order to acquire a better understanding of this organ.

2.1.1 Heart's anatomy

The heart is centred in the thorax between both lungs. Its structure could be considered as vertical symmetric and its shape seems like an inclined pyramid where the base is positioned up and the peak is positioned down to the left.

In Figure 1 is shown that the heart is divided into two parts, right and left. Each part contains a top chamber, atrium, and a bottom chamber, ventricle. Blood goes into the heart through the atriums conducted by veins: pulmonary vein, in the heart left side and superior vena cava, in the right side.

Both chambers are connected by a one-way cardiac valve which allows blood fluxes from atriums to ventricles in specific situations. The tricuspid valve is located in the heart's right side and mitral valve in the left one. Furthermore, there are other valves preventing blood to come back to the ventricles once it has been bombed: pulmonary valve which connects the right ventricle to pulmonary arteries and aortic valve which connects the left ventricle to the aorta.

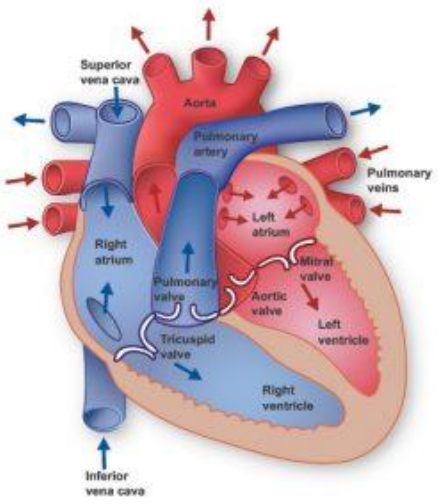

Figure 1: Human heart's anatomy Source: https://www.texasheart.org/heart-health/heart-information-center/topics/heart-anatomy/

2.1.2 Heart's principal function

As mentioned, the principal function of the heart consists in providing the fundamental nutrients to every single cell from the blood transported and remove the wastes they produce.

Two circulatory circuits, shown in Figure 2, which are dependent on each other, are found in order to accomplish heart's aim. The systemic circulation is the one in charge of providing oxygenated blood which contains the nutrients to supply the cells in every peripheral organ. It starts from the left ventricle contraction where the oxygenated blood is bomb to the aorta and because of the blood vessels size reduction to capillaries, the blood is able to arrive at every single cell. The pulmonary circulation is the circuit through the lungs where blood is oxygenated. Deoxygenated blood gets into the heart through the right atrium and the contraction of the right ventricle bomb the blood to the lungs where the wastes are eliminated and blood is oxygenated again.

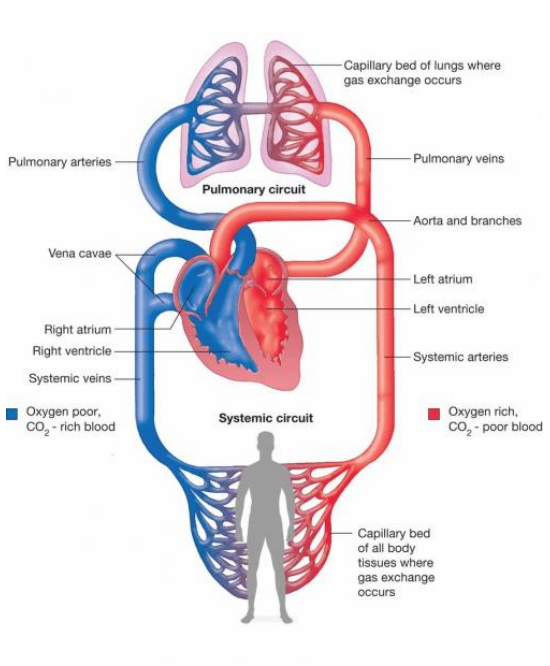

Figure 2: Systemic and pulmonary circuits. Source: https://biology-forums.com/index.php?action=gallery&sa=view&id=8516

Both, systole and diastole, shown in Figure 3, are the phases involved in the mechanism described. The systole is linked to the ventricle contraction in which the blood is bombed to one or another destination. However, a relaxation period is needed to let the blood get into the atrium, the diastole.

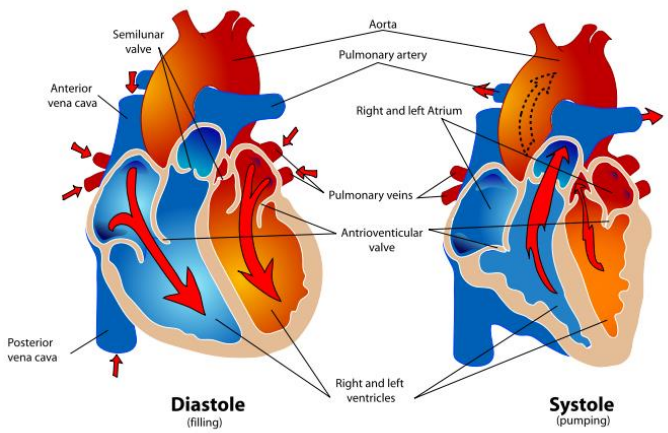

Figure 3: Systole and diastole representation. Source: https://www.differencebetween.com/difference-between-systole-and-diastole/

2.1.3 Physiology of the cardiac muscle

Three different cardiac muscles are found in the heart: auricular muscle, ventricular muscle and muscular fibres specialized in excitation and conduction.

On one hand, the auricular and ventricular muscle make the heart contraction similar to skeletal muscle and it aims to bomb the blood. The cells forming this tissue are characterized by the presence of two proteins responsible for cardiac contraction and relaxation: actin and myosin.

On the other hand, while the muscular fibres specialized in excitation are characterized by automatic electrical discharges displayed as action potentials which initiate heart contraction, the ones specialized in conduction are in charge of conducting this electrical impulse though all the heart and making contraction possible. This capacity controls the heartbeat rhythm as the cardiac contraction is initialized by these electrical impulses.

It is important to remark that the heart is considered as multiple cardiac cell syncytium. In fact, two syncytiums could be considered, auricular and ventricular, which are separated by the atrioventricular node. The high connection of the cells which form the muscle is capable to conduct the excitation of one cell to the whole organ and make the heart work as a unique cell. This connection is due to the presence of the intercalated disks, shown in Figure 4, which are communicant channels that allow rapid communication between neighbourhood cells. [1]

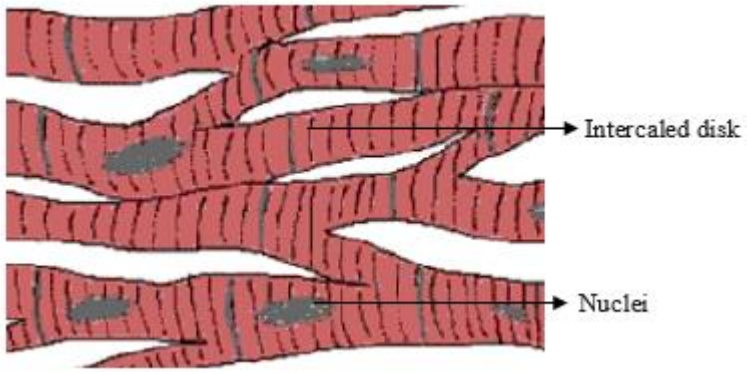

Figure 4: Cardiac muscle fibres. Source: adapted from http://tea.uwe.ac.uk/rcp/cs-heart.aspx

2.1.4 Pacemaking activity and conduction

The heartbeat rhythmicity is based on the pacemakers' cells. Specific mechanisms are capable of producing automatic action potential in specific located cells. These action potentials will be propagated to the neighbourhood cells in order to generate heart's contraction through an electrical circuit shown in Figure 5.

Pacemakers' cells are mostly found in the sinoatrial node (SAN) which is located in the intercaval region of the right atrium [2]. In this regard, SAN is considered the natural pacemaker because it is responsible for the origin electrical impulse which will lead to cardiac contraction and controls heartbeat rate.

However, another pacemaker node exists, just in case, SAN node does not work properly. This is atrioventricular node (AVN) which is located a little below the SAN, in the triangle of Koch, between the left atrium and the right ventricle within the atrial septum [2]. This node is also called the secondary pacemaker because it only will take over the pacemaker responsibility if SAN fails. It has to be taken into account that this node accomplish also with a filter function controlling the propagation velocity. The importance of this function relays on the separation between atriums and ventricles and the electrical impulse modulation just in case atrium fibrillation appears.

The electrical conduction system of the heart is the path that the action potential generated in one of the two pacemaker nodes (mostly in SAN) will follow to propagate the electrical stimulus and excite the rest of cardiac cells in order to get the contraction. This system is formed by the bundle of His which divides itself into two branches, one for its heart's side, and the Purkinje fibres which arrive at every single part of each ventricle. The cells which form this electrical system also have pacemaker activity but its rate is considerably lower than both SAN and AVN. Therefore, if both principal pacemaker nodes fail to function, these cells are capable of initializing the action potential which would lead to cardiac contraction. Nevertheless, the velocity propagation of these cells is really elevate.

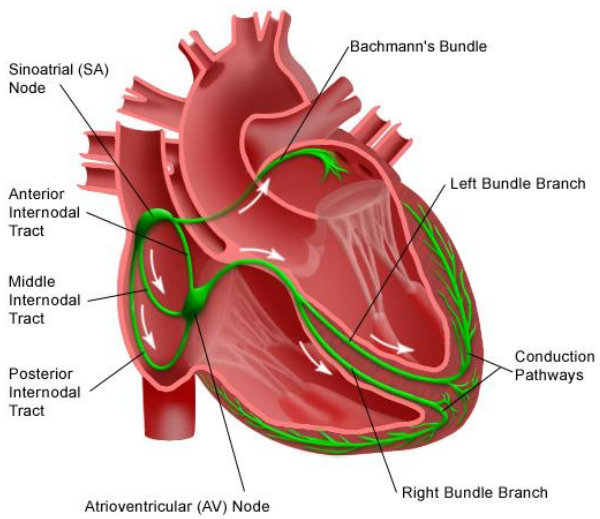

Figure 5: Electrical System of the Heart. Source: https://mdmedicine.wordpress.com/2011/04/24/heart-conduction-system/

2.2 CARDIAC CELL ELECTROPHYSIOLOGY

The cardiac electrophysiology is related to all processes which are involved in the heart's electric activation. This section will be focused on the explanation of a cardiac cell electrical representation.

2.2.1 Cell membrane

The cell membrane is the biological barrier that separates the interior of the cell from the extracellular space. It is composed of a lipid bilayer in which different proteins are embedded. Its principal function is to control both substances, entrance and exit of the cell. That's why it has some permeability to ions and organic molecules. The proteins which are located in the membrane help to control these movements and they correspond to ionic channels, bombs, exchangers or cotransporters.

Electrically, the cell membrane works such as a capacitor because of its insulating performance between both spaces intracellular and extracellular, it is separating. Therefore, it has associated a membrane capacitance (C_m) which is expressed in units of Farads (F) and it is proportionally linked to the membrane surface and its dielectric properties. Figure 6 shows an electrical representation of the cell membrane.

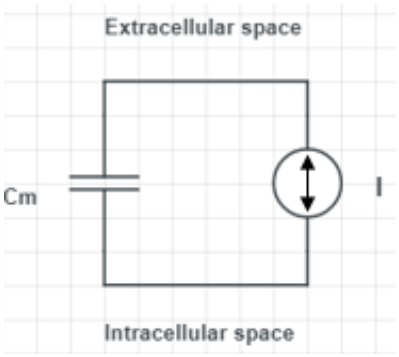

Figure 6: Representation of a simplification of the electrical circuit of a cell membrane. Source: Own elaboration.

2.2.2 Ionic channels and its modelling

The electrical activity of the cell is regulated by the movement of different ions (Na^+, Ca^{+2}, K^+, Cl^-) through the membrane.

These ions are found in different concentrations in both extracellular and intracellular space. Therefore, a force that will try to equalise their concentration in both sides of the cell membrane exits and it is called concentration gradient. Moreover, ions are characterised by being electrically charged which leads us to the second force, the electrical gradient whose aim is to have no difference electrical between both spaces.

Table 1: Extracellular and intracellular concentration of the ions.[1]

	Extracellular concentration (mM)	Intracellular concentration (Mm)
Na^+	142	10
Ca^{+2}	2.4	0.0001
K^+	4	140
Cl^-	103	4

As it is shown in Table 1 motivated by the concentration gradient sodium, calcium and chorine currents will be inward currents and potassium will be an outward current. Although this force remains constant, the electrical gradient depends on the changing cell voltage, during rest or action potential, and this will determine the direction the ions move through the membrane, as shown in Figures 7 and 8.

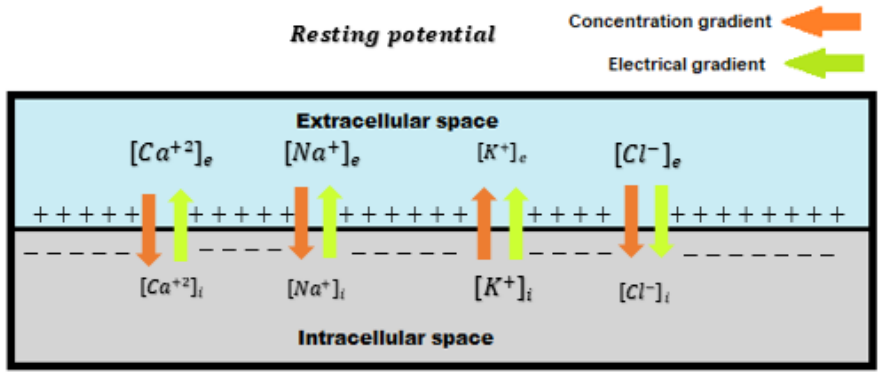

Figure 7: Trend of ion movement in the resting potential. Source: Own elaboration.

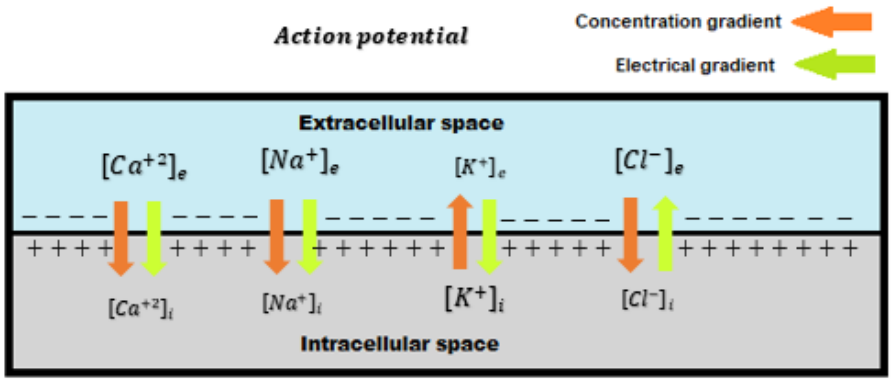

Figure 8: Trend of ion movement in the action potential. Source: Own elaboration.

It is also important to know the different kinds of transport that exist through the cell membrane. Passive transport doesn't need energy and it could be done through the lipid bilayer where the acting force is the concentration gradient but also through specific ionic channels where both forces previously explained make the transport possible. Active transport needs energy in terms of adenosine triphosphate (ATP) because these proteins work against the concentration gradient. It is important to highlight the NaK pump which gets out of the cell three sodium ions and gets in it two potassium ions, the ion movement sum makes this current an outward one, and the $NaCa$ exchanger which gets in three sodium ions and gets out one calcium ion, the ion movement sum makes this current an inward one.

Ions channels are responsible to let ions go into and out the cell and there are specific channels for each ion. However, they are not always open which means the ion flux depends on the cell situation. Therefore, ionic channels are characterized by two properties. The first one is the selectivity which means they will not allow transporting every single ion but a specific one. The second one is the gating propriety which will determine if the channel is opened or closed and only in an open state ion movement will be possible.

Ions channels have been classified because of their gating mechanism and it could be based on electrical (voltage), chemical (ligand) or mechanical (stretch) stimuli. It is said that a voltage-dependent channel is opening or closing depends on the membrane voltage.Na, Ca and different types of K currents are considered voltage-gated. Opening and closing properties in ligand channels are motivated by the intracellular or extracellular presence of a substance. That is found in some K currents.

Although gating phenomenon is complex and only partially understood, it could be understood as a conformation change in the channels in which it can reach three states: closed, open or inactivated. That means, no ion flux will appear unless the channel is open.[3]

From an electrical point of view, an ion channel could be represented such as variable resistance, shown in Figure 9, because of its dependence on voltage gradient (∇u) which is between intracellular (u_i) and extracellular (u_e) space.

$$\nabla u = u_i - u_e \tag{2-1}$$

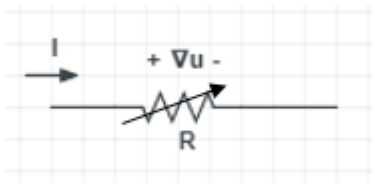

Figure 9: Electrical representation of an ion channel. Source: Own elaboration.

On one hand, Fick law could be related to concentration flux ($\overrightarrow{J_{D,s}}$) in this way:

$$\overrightarrow{J_{D,s}} = -z_S F R T u_S \overrightarrow{\nabla C_S} \tag{2-2}$$

where z_S is the number of electrons transferred by each ion S, F is the Faraday constant, R is the gas constant, T is the temperature, u_S is the ion mobility and $\overrightarrow{\nabla C_S}$ is the concentration gradient of the S ion.

On the other hand, electrical flux ($\overrightarrow{J_{E,s}}$) could be explained by Ohm's law in this way:

$$\overrightarrow{J_{E,s}} = -z_S^2 F^2 C_S u_S \overrightarrow{\nabla u} \tag{2-3}$$

where z_S is the number of electrons transferred by each ion S, F is the Faraday constant, C_S is the concentration of the ion S, u_S is the ion mobility and $\overrightarrow{\nabla u}$ is the voltage gradient.

As it has been commented, the direction of the ion current ($\overrightarrow{J_S}$) will be determined by the sum of both forces. It is important to highlight that the criterion selected determines negative currents as outwards ones.

$$\overrightarrow{J_S} = \overrightarrow{J_{D,s}} + \overrightarrow{J_{E,s}} = -u_S F z_S (R T \overrightarrow{\nabla C_S} + F z_S C_s \overrightarrow{\nabla u}) \tag{2-4}$$

It is called reversal potential (E_S) to the potential which makes no transport for a specific ion: both gradients are equal but signed differently. That term can be calculated using the Nernst law:

$$E_S = \frac{RT}{z_S F} \ln \frac{[S]_e}{[S]_i} \tag{2-5}$$

where z_S is the number of electrons transferred by each ion S, F is the Faraday constant, R is the gas constant, $[S]_e$ and $[S]_i$ are the extracellular and intracellular concentration for ion S.

Therefore, the ion current (i_S) which flows through an individual channel is defined:

$$i_S = \frac{z_S^2 F^2}{\int_i^e \frac{dx}{Ac(x)u(u)C_s(x)}} (V_m - E_s) = \gamma_S (V_m - E_s) \tag{2-6}$$

However, we are not interested in the current that flows in a single ion channel but in the whole population for that kind of channels. That could be expressed by considering the probability of the channels to be opened in front of the whole population which is a time and voltage function, $f_S(Vm, t)$. Moreover, at this point, it is also important to consider the ion conductance (G_S) which is defined as:

$$G_S(V_m, t) = N_S \gamma_S(V_m) f_S(Vm, t) \tag{2-7}$$

where N_S is the whole population for S ions channels and $f_S(Vm,t)$ is defined such as $\frac{N_{open,S}(V_m,t)}{N_S}$.

The opened channels rate can be calculated:

$$\frac{df_S}{dt} = \alpha_S(1 - f_S) - \beta_S f_S \qquad (2\text{-}8)$$

In this formula α_S represents the open rate while β_S the close rate and they also depend on V_m. The opened channels rate, f_S, can oscillate from 0 to 1.

There are two more formulas which determine ionic channels behaviour: f_{inf}, a variable related to the final number of opened channels, and τ_f, the time constant that determines how much time is needed to arrive at that final state.

$$f_{inf}(Vm) = \frac{\beta_S}{\alpha_S + \beta_S} \qquad (2\text{-}9)$$

$$\tau_f(Vm) = \frac{1}{\alpha_S + \beta_S} \qquad (2\text{-}10)$$

At this point, it is obtained:

$$\frac{df_S}{dt} = \frac{f_{inf}(Vm) - f_S}{\tau_f(Vm)} \qquad (2\text{-}11)$$

Therefore, an ion current description is established like:

$$I_S = g_S\,(Vm,t)(V_m - E_S) \qquad (2\text{-}12)$$

where the conductance (g_S) of the ion S depends on the voltage and time.

2.2.3 Cell electrical model

At this point, it can be understood a complete electrical representation of the cellular behaviour where all the families' ionic channels and membrane cells are considered, shown in Figure 10.

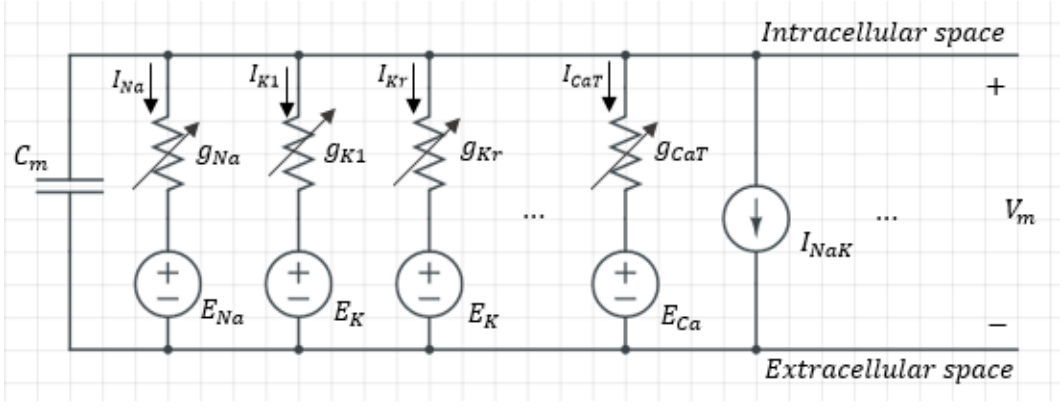

Figure 10: Cell electrical representation. Source: Own elaboration.

Finally, this electrical model could be expressed with just one equation representing the cell electrophysiology performance:

$$\frac{dV_m}{dt} = -\frac{1}{C_m} I_X \qquad (2\text{-}13)$$

$$I_X = \sum_S I_S + \sum_{B,I} I_{B,I} + I_{stim} \qquad (2\text{-}14)$$

I_X includes all the existence currents in the cell: the ones from the ionic channels ($\sum_S I_S$), the ones from active transport ($\sum_{B,I} I_{B,I}$) and the stimulation current (I_{stim}) in case it exists.

2.3 ACTION POTENTIAL

The definition of an action potential (AP) could be the electric impulse which is received by a single cell and provokes a modification of its voltage. The AP of a cardiac ventricular myocyte has been largely studied and it will be used as a reference to understand the differences between SAN and AVN cells.

As shown in Figure 11, the AP of a cardiac ventricular myocyte presents four different phases. The phase 0 corresponds to the action potential upstroke. The membrane potential remains constant since a stimulus appears which is able to increase the membrane potential to the threshold potential (around -65 mV). At this moment, sodium channels open and this inward current makes the potential rapidly become less negative, this process is known as cell depolarization. When the membrane potential reaches -40 mV, L-type calcium channels also start to open and another inward current appears. However, I_{Na} is a really brief current due to its fast kinetics, as it can be observed in Figure 11 where its shape seems like a spike, and after a few milliseconds the sodium channels stop their conduction, they close. The membrane potential has reached +20mV at the end of this phase.

Then, there is a rapid repolarization which corresponds to phase 1. At this moment, the sodium channels have mostly inactivated and the potassium currents are the ones that are taken into account turning on. Therefore, there is an outward current, I_{to}, which makes the membrane potential rapidly decrease. However, there is not a complete repolarization due to the presence of calcium currents which are still activated due to their slow kinetics. During several milliseconds both outward potassium currents and inward calcium currents are activated. Therefore, the membrane potential remains considerably constant for a while. This corresponds to phase 2 and it is called the plateau.

Phase 3 corresponds to the complete repolarization since the calcium currents have inactivated while potassium ones remain active, so the membrane potential decreases. At the beginning of this phase, I_{Kr} is the responsible potassium current but then I_{Ks} appears. It has the same function but its kinetics are slower.

Finally, phase 4 is called the diastolic phase where the membrane potential remains constant at approximately -80mV. This is called resting potential and it corresponds to the potassium reversal potential because the only ionic channel which remains open is a potassium one (I_{K1}). [3]

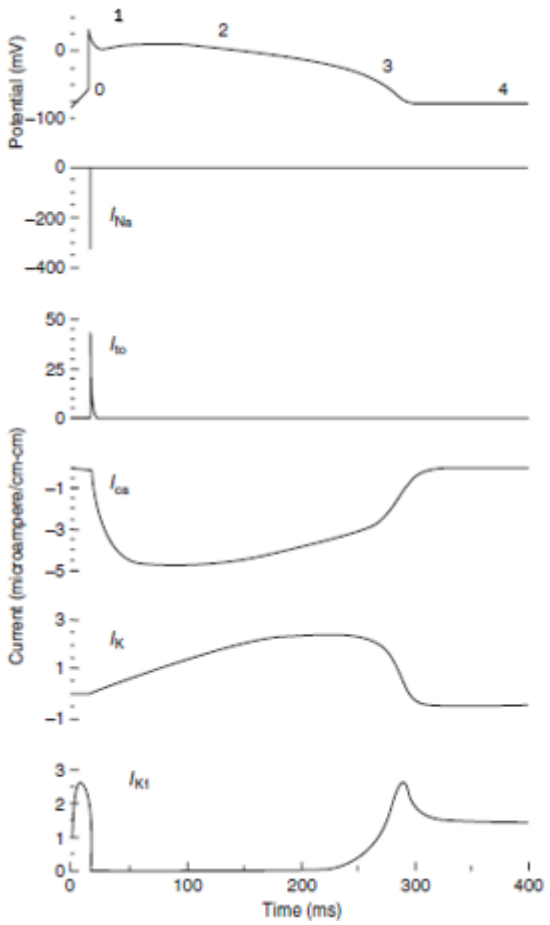

Figure 11: Action potential from a cardiac ventricular myocyte. [3]

2.3.1 Characteristics of SAN and AVN action potential

Some differences are found between the AP previously explained and the one that presents SAN and AVN cells, shown in Figure 12.

As mentioned before, SAN cells are the ones responsible for cardiac activation. Therefore, the diastolic membrane potential does not remain constant because a slow depolarization brings the membrane potential to the activation threshold in order to get the following AP. This phenomenon occurs because of the presence of I_f, an inward current activated by hyperpolarization which only appears in pacemaker's cells. Moreover, the maximum diastolic potential is less negative (between -50 and -65 mV) than in the AP previously explained. This fact is due to the lower permeability to potassium that SAN cells have in front of ventricular ones what makes the maximum diastolic voltage less negative. Furthermore, we can observe that there are neither phase 1 nor phase 2 which means in these cells there is not I_{to} and calcium current is not so persistent in time as their contractile function is not as important as in ventricular myocyte. However, calcium currents are responsible for the upstroke in the cell's depolarization which makes the upstroke velocity slower. [3]

AVN is the second pacemaker and also this fact is reflected in the AP that its cells generated. The maximum diastolic potential is less negative than in the ventricular cells and its action potential upstroke is slower and mostly dependent on calcium current. As shown in Figure 12, AVN action potential consists of the four phases described in the ventricular myocyte. Although AVN has pacemaker activity, its frequency is lower. Therefore, it will be capable of generating an AP, what mean I_f exists in these cells but just in case SAN fails.

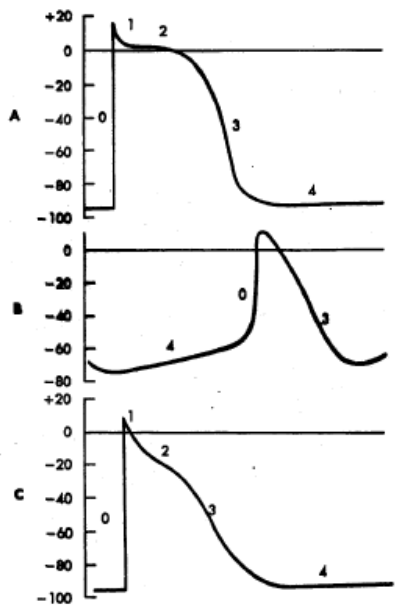

Figure 12: Action potential of a (A) ventricular cell, (B) SAN cell, (C) AVN cell. Source:Presentation of Modelli e Metodi per la Cardiologia Computazionale by prof. Stefano Severi

2.3.2 Importance of calcium handling

Calcium ion has an important role related to the cardiac contraction. The calcium induced-calcium released (CICR) process is in charge of increasing the intracellular calcium concentration in order to carry out the cardiac contraction.

This process is based on the capacity that the intracellular calcium increase can activate the calcium release from intracellular calcium reserves. It starts from the entrance of calcium in the cell because of the depolarization of itself and the opening of the L-type calcium channels which is going to increase calcium concentration in the intracellular space. Ryanodine Receptors (RyR) are located in the sarcoplasmic reticulum (SR) membrane and they are Ca^{+2} ligand-dependent which mean that an increase in calcium intracellular concentration will make them activate. This activation will allow calcium in SR exits from junctional SR (JSR) to the cytosol and increasing the intracellular calcium concentration. Calcium released is going to join T troponin which is going to provoke a tropomyosin displacement allowing the linkage between actin and myosin.

To return to the state of muscular relaxation, intracellular calcium concentrations need to decrease causing troponin I to cover the actin binding sites again. The calcium concentration will go back to normality thanks to the action of the SERCA, sarco/endoplasmatic reticulum Ca^{+2}-ATPase, bomb which will introduce calcium inside the network SR (NSR) and the $NaCa$ exchanger which will push out calcium to the extracellular space while three sodium ions entre to the cell.

CHAPTER 3: **OBJECTIVES**

This master thesis is a continuation from the work done by Matteo Mangoni which consists of the development of an action potential mouse AVN single-cell model which will include calcium handling. Therefore, the principal objective of this master thesis is to develop a code capable of simulating the action potential of a mouse AVN single cell with calcium dynamics consideration. Accordingly, the objectives of this work are:

- Introduce calcium handling equations to the action potential mouse AVN single-cell model and adapt them to obtain a well-working and physiological model.
- Reformulate AVN ionic currents to have a better approach to reality based on a Voltage-Clamp fitting from experimental data.
- Include the action potential mouse SAN single-cell model in the presented model in order to be able to simulate SAN or AVN model by changing a flag.

CHAPTER 4: **METHODS**

4.1 PREVIOUS WORK

This work aims to introduce calcium handling equations to an action potential mouse AVN single-cell existing model. This preliminary work was started by Matteo Mangoni at the *Centre National de la Recherche Scientifique*, Montpellier, using XPP programming and then translated to MatLab language by a graduate student. Therefore, this software was able to simulate an action potential mouse AVN single cell without considering neither cell's compartmentalization nor dynamic intracellular concentrations. It is shown a cell's representation of the considered model in Figure 13.

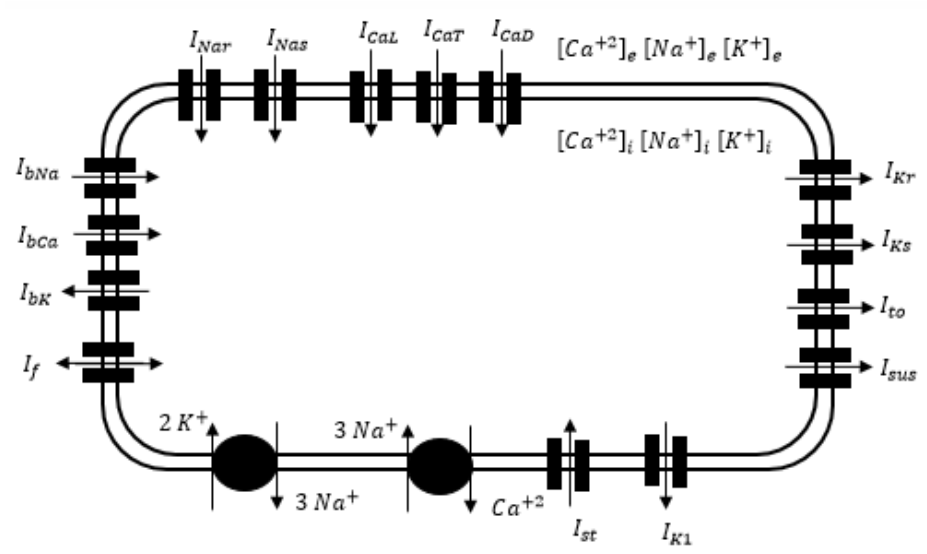

Figure 13: Schematic diagram of the mouse AVN single cell preliminary model. Source: Own elaboration.

The equations which describe calcium handling were taken from the AP mouse SAN single-cell model done by Matteo Mangoni in JSim programming. Calcium handling equations from this model are based on Kharche's work [4]. It is shown in Figure 14 the cell's representation for this model.

The presented model considers cell's representation showed in Figure 14 where both AP mouse single cell model, one for SAN and the other for AVN, can be modelled. This is possible due to the introduction of a flag that allows the choice between the models. SAN model was translated from JSim programming to MatLab language and their equations for calcium dynamics were introduced in the existing AVN model.

There were needed some unit changes in AVN model as it was expressed in mV/s while SAN model was expressed in mV/ms. It was decided to express the resulting model in mV/ms because it is a more consistent unit result.

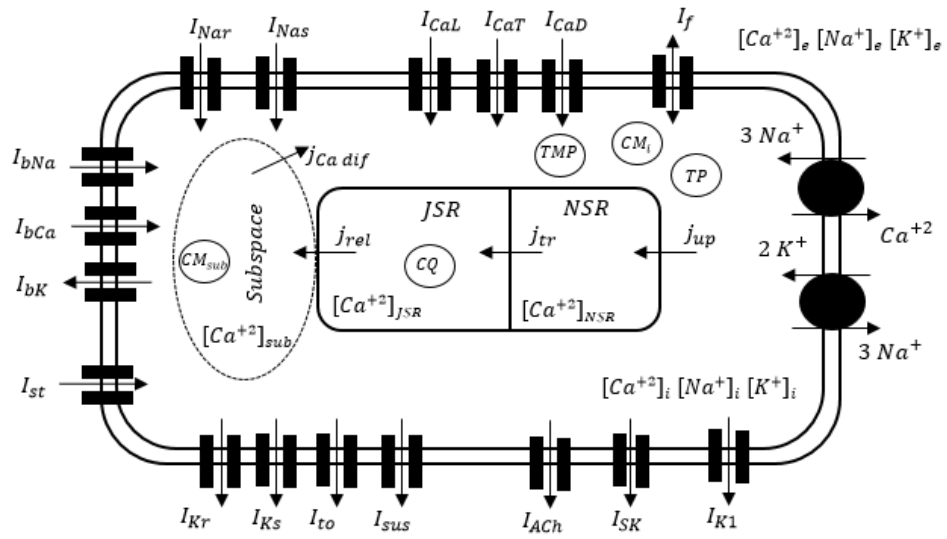

Figure 14: Schematic diagram of the mouse SAN single cell model. Source: Own elaboration.

4.2 THE MODEL DEVELOPED

The presented model can reproduce the AP of a mouse SAN and AVN cell. Simulations were carried out on an Acer Aspire E5-573G computer using MatLab programming. While the mouse SAN cell model consists of 40 state variables, the mouse AVN cell consists of 39. A nonlinear ODE system has been used such as the integration method in both models, specifically *ode15s* from MatLab with a constant step time ($dt = 1\ ms$).

As mentioned, the action potential model is measured in mV/ms. Furthermore, current results are presented as current density measured in pA/pF due to the link between maximal conductance for each ion and cell capacitance.

The structure of the presented model, shown in Figure 15, is based on two functions which are called *main* and *model*, they can be found in the *Appendix*. The function *model* is the one where all the constants, variables and mathematical equations are described to reproduce SAN or AVN single cell electrophysiology. Its input consists of the initial values for the variables that are going to be modelled (Y), the simulation time ($time$) and the flag which determines SAN or AVN cell ($mflag$). Its output consists of a vector time (t) and a matrix where each column corresponds to each state variable and each row corresponds to the associated time value (Yc).

The function *main* is the one in charge of controlling the simulation process and sharing the information obtained. Here, the initial values for the state variables are defined and the flag for choosing between SAN or AVN model is described.

Another function, called *parameters*, is used in order to calculate the biomarkers of the action potential which will be used to evaluate the model. This function needs the time (t), the membrane voltage (V_m) and the total ionic current (I_{tot}) as inputs and its output consists of four biomarkers, see below.

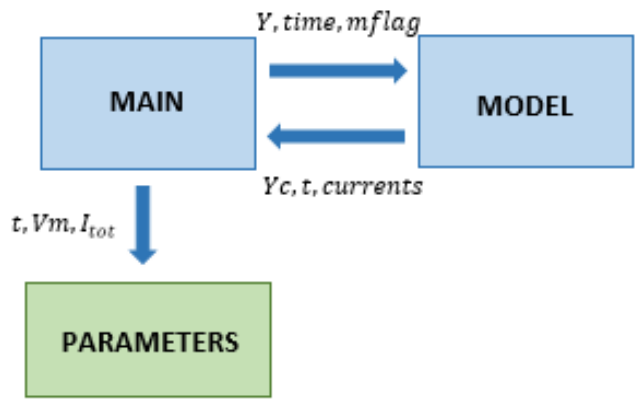

Figure 15: Workflow of the presented model. Source: Own elaboration.

It is shown in Figure 14 a schematic representation of what elements are included in the presented model. One principle change from the previous model is the cell's compartmentalization. In this model, four compartments are considered: the sarcoplasmic reticulum, divided in junctional and network spaces, the calcium subspace and the cytosol. The calcium subspace is considered as a different cell compartment because of the different calcium concentration found when the release takes place.

In the previous mentioned models, I_{bK} and I_{bCa}were not included in the description of I_X because it was not clarified its presence in SAN cell. Nevertheless, it has been demonstrated its existence has been supported by recent results from Mangoni's lab and they have been taken into account the current total sum. Therefore, I_X is defined as the sum of these transmembrane ionic currents:

$$I_X = I_{Na} + I_{Nas} + I_{CaL} + I_{CaT} + I_{CaD} + I_{K1} + I_{Kr} + I_{Ks} + I_{to} + I_{sus} + I_f + I_{bNa} + I_{bK} + I_{bCa} + I_{st} + I_{SK} + I_{KACh} + I_{NaK} + I_{NaCa} + I_{stim} \quad (4\text{-}1)$$

- I_{Na}, inward resistant component of Na^+current
- I_{Nas}, inward sensitive component of Na^+current
- I_{CaL}, inward Ca^{+2} current through L-type $Ca_{1.2}$ channels
- I_{CaD}, inward Ca^{+2} current through L-type $Ca_{1.3}$ channels
- I_{CaT}, inward Ca^{+2} current through L-type $Ca_{3.1}$ channels
- I_{K1}, inward rectifier time-independent K^+ current
- I_{Kr}, outward rapid delayed rectifier K^+ current
- I_{Ks}, outward slow delayed rectifier K^+ current
- I_{to}, outward transient K^+ current
- I_{sus}, outward sustained K^+ current
- I_f, Na^+ and K^+ currents activated by hyperpolarization
- I_{bNa}, Na^+ background current
- I_{bK}, K^+ background current
- I_{bCa}, K^+ background current
- I_{st}, inward sustained
- I_{SK}, Ca^{+2}-activated K^+current
- I_{KACh}, background muscarinic K^+ current
- I_{NaK}, resulting current from the NaK pump
- I_{NaCa}, resulting current from the $NaCa$ exchanger
- I_{stim}, current generated by the cardiac stimulus

I_{stim} is not present in SAN model I_X description because of its primary pacemaker function and it is there where this current is originated. In AVN model, this current represents the electric impulse generated in SAN which aim is to depolarize all the heart. As mentioned before, if I_{stim} is not generated in SAN, AVN can do it but with a lower heart rate.

4.3 BIOMARKERS FOR MODEL EVALUATION

Once a consistent and working model is obtained, some experimental biomarkers will be used to support our results. Two references, Table 2 and Table 3, will be used to evaluate the presented model. These biomarkers are the following ones and they are schematically shown in Figure 16.

- Rate: The rate is defined as the times an AP appears in a determinate temporal distance. In this work, it will be measured as beats per minute (bpm).
- Maximum diastolic potential (MDP): The MDP is the minimum potential during the diastolic phase and it is measured in mV.
- Action potential amplitude (APA): The APA is the absolute difference from the MDP to the maximum value AP reaches, V_{max}, and it is measured in mV.
- Action potential duration (APD): The APD is the time, measured in ms, that elapses between the start of the AP and the end of the repolarization of that AP. It could be considered different $APDs$: APD_{90}, APD_{70}, APD_{50} and APD_{30} action potential duration when 90%, 70%, 50% and 30%, respectively, of the membrane voltage have been repolarized.

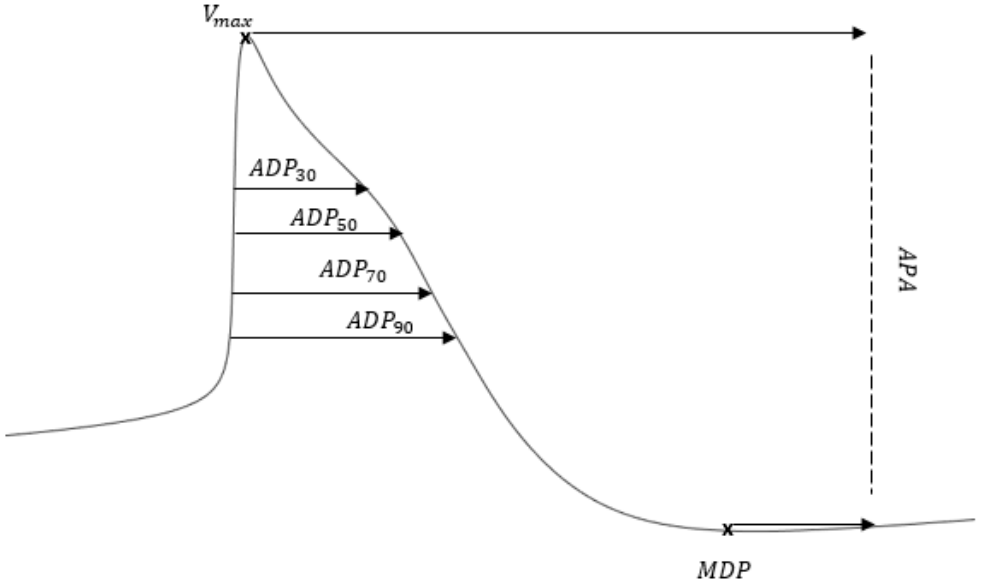

Figure 16: Representation of the AVN biomarkers. Source: Own elaboration.

Table 2: AVN biomarkers [5]

	AVN
$\boldsymbol{Rate\ (bpm)}$	173 ± 27
$\boldsymbol{MDP(mV)}$	-57 ± 1
$\boldsymbol{APA(mV)}$	91 ± 7

Table 3: AVN biomarkers [6]

	AVN
$\boldsymbol{MDP(mV)}$	-62 ± 1
$\boldsymbol{APA(mV)}$	76 ± 3
$\boldsymbol{APD_{30}(ms)}$	25 ± 4
$\boldsymbol{APD_{50}(ms)}$	37 ± 6
$\boldsymbol{APD_{70}(ms)}$	60 ± 6
$\boldsymbol{APD_{90}(ms)}$	100 ± 8

CHAPTER 5: MODEL DEVELOPMENT

This chapter aims to present all the modifications considered to improve the preliminary AVN model and convert it to a second generation one by considering calcium handling which involves cell compartmentalization and dynamic ionic intracellular concentrations. Furthermore, it also exposed the different current reformulation based on AVN experimental data.

5.1 Cell dimension reformulation

It was needed to link the cell dimension and membrane capacitance to a characteristic AVN cell. The cell dimension description was maintained as a cylindrical structure where length and radius of the cell were linked to the membrane capacitance. This objective was accomplished by fixing both membrane capacitance to 22 pF, as reported in experimental data [5] [6], the cell radius to 5 μm and the cell length was calculated using the cylindrical description and the membrane capacitance predefined $\frac{1uF}{cm^2}$.

5.2 Calcium handling introduction

The principal objective of this work was the introduction of the calcium handling to the mouse AVN single cell model. This implementation took into account cell's compartmentalisation, dynamic ionic intracellular concentration (Na_i^+, Ca_i^{+2}, K_i^+) and calcium buffering. The equations introduced were the ones used in AP mouse SAN single-cell model which are taken from Karche's model [4].

On one hand, calcium dynamics introduction leads to a cell's compartmentalisation as it is shown in Figure 14. The compartmentalisation of the cell is based on three new subspaces apart from the cytosol. Two of these new subspaces are related to the sarcoplasmic reticulum which is divided into the junctional (JSR) and the network (NSR). JSR is the space where calcium is accumulated and from where it goes to the cytosol in the calcium release, it is described as the 1.12% of the whole cell volume. However, the NSR is the space where calcium goes in its uptake and it is described as the 11.6% of the whole volume cell. The other subspace created is not a really existence cell compartment but a part of the cell cytosol. It is situated next to the JSR and the importance of its existence resides in the different calcium concentration that this part of the cytosol will have when calcium releases from JSR. This subspace is considered 0.1% of the whole cell volume. It is also important to take into account that the intracellular space is described as the subtraction of the 46% whole volume cell and the subspace previously explained. The rest of the cell volume is considered occupied by cellular organelles.

Because of subspaces existence, four fluxes related to calcium handling appear in the model: j_{up} is linked to SERCA pump which is in charge of taking Ca_i^{+2} from the cytosol to the NSR in order to reestablish intracellular calcium concentration, j_{tr} is the flux between NSR and JSR, j_{rel} is associated with calcium release from JSR to the cytosol subspace induced by the intracellular calcium concentration increase during the AP upstroke and $j_{Ca_{dif}}$ is the calcium diffusion from the cytosol subspace to the whole cytosol. The following equations describe their behaviours:

$$j_{up} = \frac{P_{up}}{1 + \frac{K_{up}}{Ca_i}} \quad (5\text{-}1)$$

$$j_{tr} = \frac{Ca_{NSR} - Ca_{JSR}}{\tau_{tr}} \quad (5\text{-}2)$$

$$j_{rel} = ks * O1 * (Ca_{JSR} - Ca_{sub}) \quad (5\text{-}3)$$

$$j_{Ca_{dif}} = \frac{Ca_{sub} - Ca_i}{\tau_{Ca_{dif}}} \quad (5\text{-}4)$$

where P_{up} is the rate constant of Ca^{+2} uptake expressed in mM/ms, K_{up} is the half-maximal $[Ca^{+2}]_i$ of Ca^{+2} uptake expressed in mM, τ_{tr} is the time constant for j_{tr} expressed in ms, ks is the Ca^{+2} release constant expressed in $1/ms$, $\tau_{Ca_{dif}}$ is the time constant for $j_{Ca_{dif}}$ expressed in ms and ks is the release parameter. $O1$ is the open state for RyR from a release Markovian description taken from Kharche's model [4].

Calcium located in the cytosol is considered physiological when its concentration is not superior to 1 μM. For this reason, intracellular and subspace calcium initial concentration values were considerably reduced because they were defined highly superior to 1 μM and they established such as $[Ca^{+2}]_{i_{initial}} = 0.0326892\ uM$ and $[Ca^{+2}]_{sub_{initial}} = 0.0534741\ uM$.

On the other hand, calcium buffering is also considered. The buffers considered are: troponin Ca^{+2} site (TC) and troponin Mg^{+2} site (TMC) located in the cytosol, calmodulin located in the subspace (CM_s) and cytosol (CM_i) and calsequestrin (CQ) located in JSR. Its modelling equations are:

$$\frac{df_{TC}}{dt} = k_{f_{TC}}[Ca^{+2}]_i(1 - f_{TC}) - k_{b_{TC}}f_{TC} \quad (5\text{-}5)$$

$$\frac{df_{TMC}}{dt} = k_{f_{TMC}}[Ca^{+2}]_i(1 - f_{TMC} - f_{TMM}) - k_{b_{TMC}}f_{TMC} \quad (5\text{-}6)$$

$$\frac{df_{TMM}}{dt} = k_{f_{TMM}}[Mg^{+2}]_i(1 - f_{TMC} - f_{TMM}) - k_{b_{TMM}}f_{TMM} \quad (5\text{-}7)$$

$$\frac{df_{CMi}}{dt} = k_{f_{CM}}[Ca^{+2}]_i(1 - f_{CMi}) - k_{b_{CM}}f_{CMi} \quad (5\text{-}8)$$

$$\frac{df_{CMs}}{dt} = k_{f_{CM}}[Ca^{+2}]_{sub}(1 - f_{CMs}) - k_{b_{CM}}f_{CMs} \quad (5\text{-}9)$$

$$\frac{df_{CQ}}{dt} = k_{f_{CQ}}[Ca^{+2}]_{rel}\left(1 - f_{CQ}\right) - k_{b_{CQ}}f_{CQ} \quad (5\text{-}10)$$

where $k_{b_x}$is the pertinent ion dissociation constant of the buffer x expressed in $\frac{1}{ms}$, k_{f_x} is the pertinent ion association constant of the buffer x expressed in $\frac{1}{mM*ms}$ and f_x is the fractional occupancy of the buffer x by the pertinent ion.

Finally, as intracellular ionic concentrations are considered dynamic variables instead of states ones, the following balanced equations are included where ionic membrane currents, calcium fluxes and buffering are taken into account.

$$\frac{d[Na_i^+]}{dt} = -\left(I_{f_{Na}} + I_{st} + I_{Nas} + I_{Nar} + I_{bNa} + 3 * I_{NaK} + 3 * I_{NaCa}\right) * \frac{C_m}{F * (V_i + V_{sub})} \quad (5\text{-}11)$$

$$\frac{d[K_i^+]}{dt} = -\left(I_{Kr} + I_{Ks} + I_{to} + I_{sus} + I_{SK} + I_{K1} + I_{f_K} + I_{KACh} - 2 * I_{NaK} + I_{bK}\right) * \frac{C_m}{F * (V_i + V_{sub})} \quad (5\text{-}12)$$

$$\frac{d\left[Ca_i^{+2}\right]}{dt} = -(I_{CaL} + I_{CaT} + I_{bCa} + 0.71 * I_{CaD} - 2 * 0.2 * I_{NaK} + I_{bK}) * \frac{C_m}{F * (V_i + V_{sub})} \quad (5\text{-}13)$$

$$\frac{d\left[Ca_{sub}^{+2}\right]}{dt} = -(0.21 * I_{CaD} - 2 * 0.8 * I_{NaCa}) * \frac{C_m}{F * (V_i + V_{sub})} + \frac{j_{rel} * V_{JSR}}{V_{sub}} - (j_{Ca_{dif}} + CM_{tot} * delta_{fCMs}) \quad (5\text{-}14)$$

$$\frac{d[Ca^{+2}_{NSR}]}{dt} = j_{up} - j_{tr} * \frac{V_{JSR}}{V_{NSR}} \quad (5\text{-}15)$$

$$\frac{d[Ca^{+2}_{JSR}]}{dt} = j_{tr} - (j_{rel} + CQ_{tot} * delta_{fCQ}) \quad (5\text{-}16)$$

5.3 Ionic current description and reformulation

Ionic current description was taken from the preliminary mouse AVN single-cell model for the currents described in it as Hodking-Hukley formulation. Calcium handling equations were taken from JSim model and introduce in order to develop the presented model. Also from this model, other ionic currents, I_{SK} and I_{KACh}, are included.

Experimental data [5] from mouse AVN single cell was used to reformulate different currents (I_{Nar}, I_{Nas}, I_f, I_{CaT}, I_{CaD}, I_{to} and I_{Kr}) in the presented model in order to obtain a more realistic current description. Experimental data was based on an I-V curve for each current. This curve was obtained from a different Voltage-Clamp protocol for each current where it was defined a voltage holding and different voltages test. Therefore, the presented I-V curve recorded the maximal value for the current at different voltages test.

These I-V curves were computationally reproduced by using the same Voltage-Clamp protocol for each isolated cell and the result was compared with the experimental data one. See below the different modifications to the current description that were done to fit the simulated curve with the experimental one.

5.3.1 Sodium currents

As reported in the previous work done by a graduate student, there was an error in both sodium currents, I_{Nar} and I_{Nas}, related to their activation gate *m* which needed to be corrected to reproduce a standard electrophysiological behaviour.

In the previous model, these gates did not completely open, their maximum was 1/3. This fact was not representing the sodium gating activity in a correct mode because a normal AVN cell can completely open their sodium activation gates (m) going from 0 to 1. Therefore, the equation representing m gate state was substituted by the following one:

$$m_{inf_{Nax}} = \frac{1}{1 + e^{\frac{V+V_{act_x}}{-sNa_x}}} \quad (5\text{-}17)$$

where Nax is referring to Nar or Nas, V is the voltage membrane, V_{act_x} is the half activation voltage for Nax current and sN_{a_x} is the slope factor for Nax.

Nevertheless, this reformulation directly affected the amount of sodium inward current during the AP upstroke phase. Experimental data was used to adjust different parameters in both sodium currents. It was computationally reproduced the Voltage-Clamp protocol presented in the previous experiment and the resulting I-V curves were compared with the ones reported, shown in Figures 18 and 20. The Voltage-Clamp protocol considered a voltage holding of -90 mV and different voltage test from -60 mV to 10 mV by 5 mV step including also 20 and 30 mV voltage tests, it is indicated in the Figure 17A and 19A.

This comparison led us to reduce considerably the conductance in both cases: g_{Nar} was multiplied per 0.034, g_{Nas} was multiplied per 0.066. V_{act} and sNa were also modified in both currents descriptions. In I_{Nar}, V_{act} was reduced by $3mV$ and fixed to 40 mV and sNa was modified to 3 instead of 7. In I_{Nas}, the V_{act} was increased 5 mV and fixed to 36 mV and sNa was modified to 4 instead of 4.4.

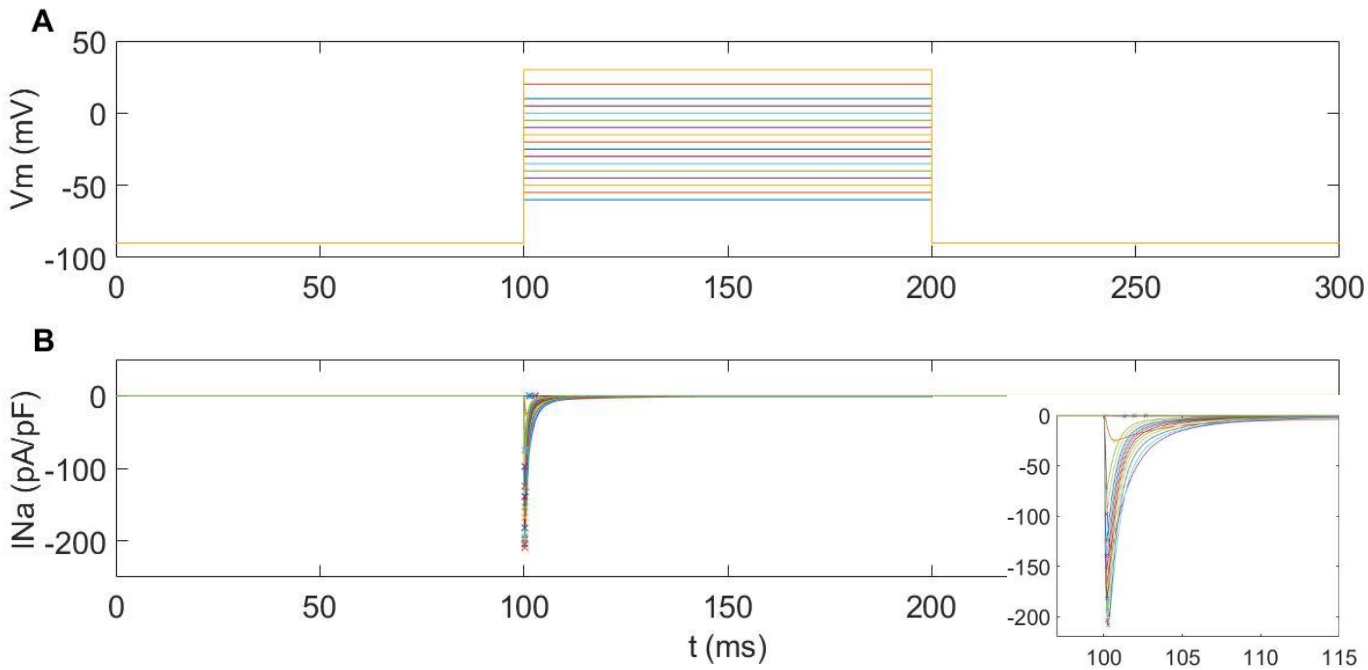

Figure 17: (A): Voltage-Clamp protocol for I_{Nar}. (B): I_{Nar} for mouse AVN single cell, maximal current values (x) and a zoom inserted to see the I_{Nar} behaviour. Source: Own elaboration.

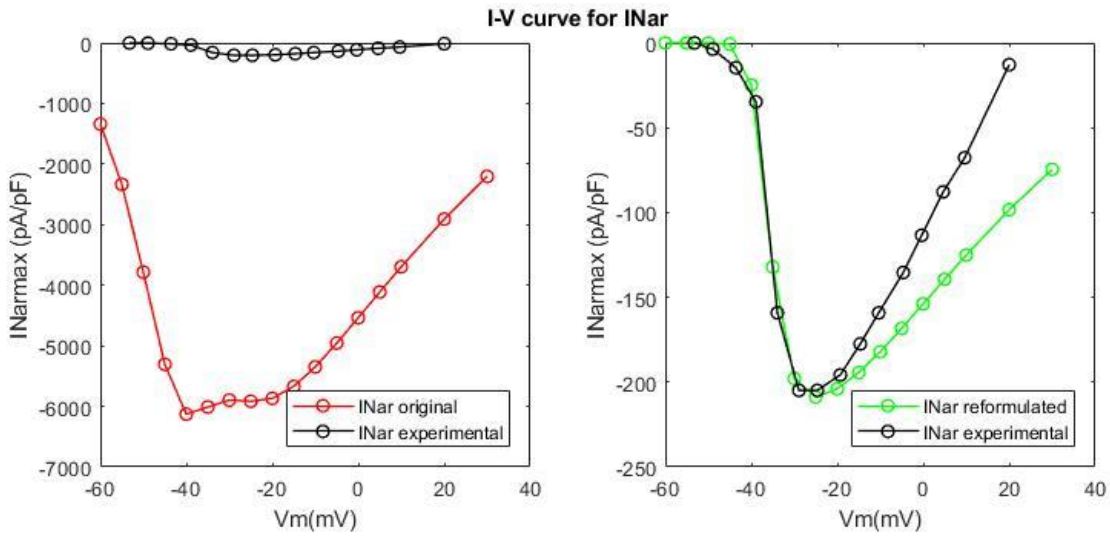

Figure 18: I-V curve for I_{Nar}. Source: Own elaboration.

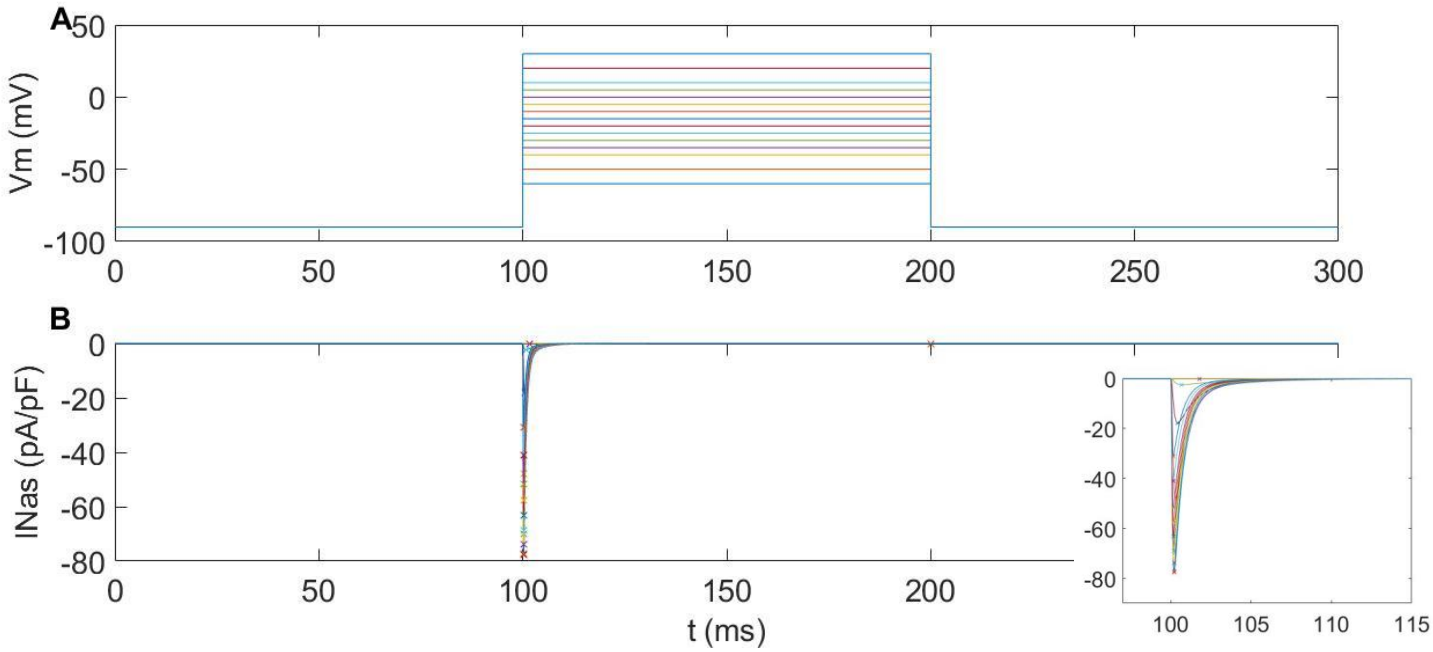

Figure 19: (A): Voltage-Clamp protocol for I_{Nas}. (B): I_{Nas} for mouse AVN single cell, maximal current values (x) and a zoom inserted to see the I_{Nas} behaviour. Source: Own elaboration.

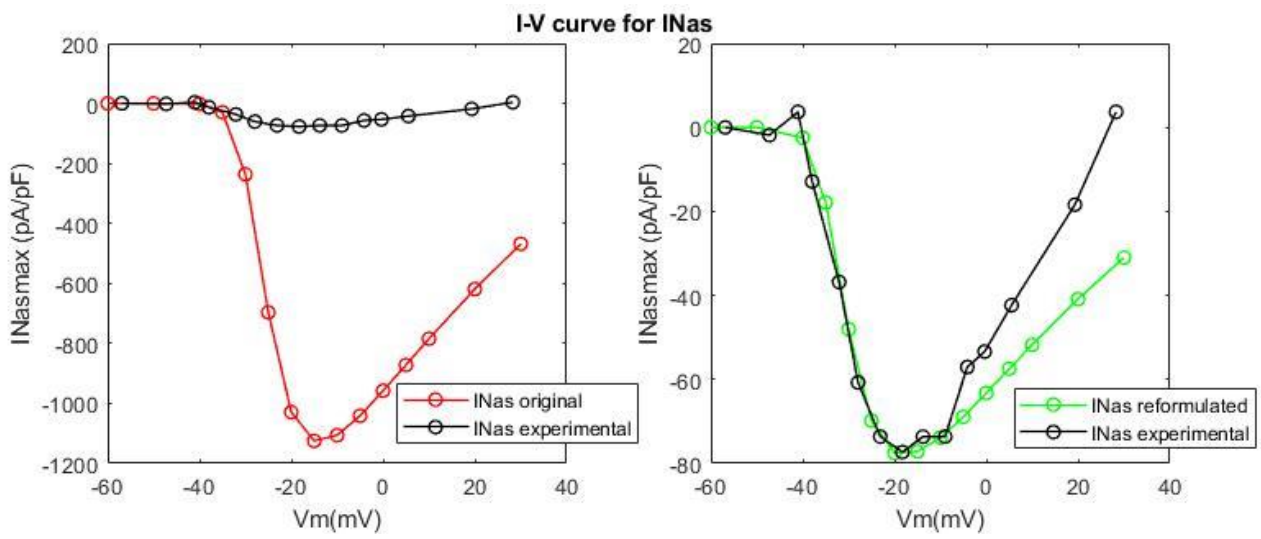

Figure 20: I-V curve for I_{Nas}. Source: Own elaboration.

No-fitting of the right part of both I-V curves was done. Reversal potential is the parameter modulating this I-V curve part and it is clearly higher in the presented model. It was calculated using the Nernst equation which is based on intracellular and extracellular sodium concentration. These concentrations are not easy to measure in experimental conditions because of the rapid kinetics of these currents. It has been decided to maintain the original concentrations and consider this no-fitting an improvement which will be taken into account when more experimental data would be available.

Both I_{Nar} and I_{Nas} are inward currents described with three gates: m and ms, an activation gate, $h1$,$h2$ and $hs1$, $hs2$, inactivation gates. Therefore, the equations which describe sodium currents are the following ones:

For I_{Nar}:

$$I_{Nar} = g_{Nar} * m^3 * h * Na_o * \frac{F^2}{RT} * \frac{e^{(V-E_{Na})*\frac{F}{RT}}-1}{e^{V*\frac{F}{RT}}-1} * V \quad (5\text{-}18)$$

$$m_{inf} = \frac{1}{1+e^{\frac{V+V_{act_r}}{-sNa_r}}} \quad (5\text{-}19)$$

$$\tau_m = \frac{0.6247}{0.832 * e^{-0.335*(V+56.7)} + 0.627 * e^{0.082*(V+65.01)}} + 0.04 \quad (5\text{-}20)$$

$$h = (1 - F_{Na}) * h1 + F_{Na} * h2 \quad (5\text{-}21)$$

$$h1_{inf} = \frac{1}{1+e^{\frac{V+V_{inact_r}}{6}}} \quad (5\text{-}22)$$

$$\tau_{h1} = \frac{0.003717 * e^{-0.2815*(V+17.11)}}{1 + 0.003732 * e^{-0.3426*(V+37.76)}} + 0.59779 \quad (5\text{-}23)$$

$$h2_{inf} = h1_{inf} \quad (5\text{-}24)$$

$$\tau_{h2} = \frac{0.00003186 * e^{-0.6219*(V+18.11)}}{1 + 0.00007189 * e^{-0.6683*(V+34.07)}} + 3.556 \quad (5\text{-}25)$$

$$F_{Na} = \frac{0.0952 * e^{-0.063*(V+34.4)}}{1 + 1.66 + e^{-0.225*(V+63.7)}} + 0.0869 \quad (5\text{-}26)$$

For I_{Nas}:

$$I_{Nas} = g_{Nas} * ms^3 * hs * Na_o * \frac{F^2}{RT} * \frac{e^{(V-E_{Na})*\frac{F}{RT}}-1}{e^{V*\frac{F}{RT}}-1} * V \quad (5\text{-}27)$$

$$ms_{inf} = \frac{1}{1+e^{\frac{V+V_{act_s}}{-sNa_s}}} \quad (5\text{-}28)$$

$$\tau_{ms} = \tau_m \quad (5\text{-}29)$$

$$hs = (1 - F_{Nas}) * hs1 + F_{Nas} * hs2 \quad (5\text{-}30)$$

$$hs1_{inf} = \frac{1}{1+e^{\frac{V+V_{inact_s}}{3}}} \quad (5\text{-}31)$$

$$\tau_{hs1} = \tau_{h1} \quad (5\text{-}32)$$

$$hs2_{inf} = hs1_{inf} \quad (5\text{-}33)$$

$$\tau_{hs2} = \tau_{h2} \quad (5\text{-}34)$$

$$F_{Nas} = F_{Na} \quad (5\text{-}35)$$

where g_{Na}, g_{Nas} are the conductance for I_{Na} and I_{Nas} expressed in nS/pF and F_{Na} , F_{Nas} are the fraction of I_{Na} inactivating slowly for I_{Na} and I_{Nas}.

Nevertheless, the introduction of I_{Na} reformulation did not allow the model to arrive at the steady-state and made cell stop beating, see in the subchapter *Final model* for further information.

5.3.2 Potassium currents

I_{Kr}

Experimental data used for I_{Kr} reformulation was based on an I-V curve, shown in Figure 22. Voltage-Clamp protocol was computationally reproduced using a voltage holding -60 mV and voltages test from -50 mV to +40 mV by 10 mV steps, shown in Figure 21A. A single modification was set up: its conductance was reduced by being multiplied per 0.34.

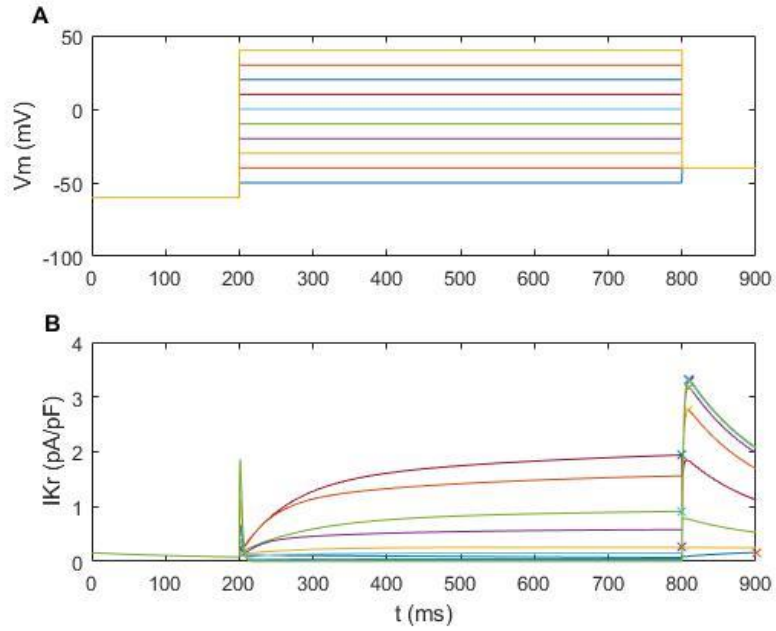

Figure 21: (A): Voltage-Clamp protocol for I_{Kr}.(B): I_{Kr} for mouse AVN single cell and maximal current values (x). Source: Own elaboration.

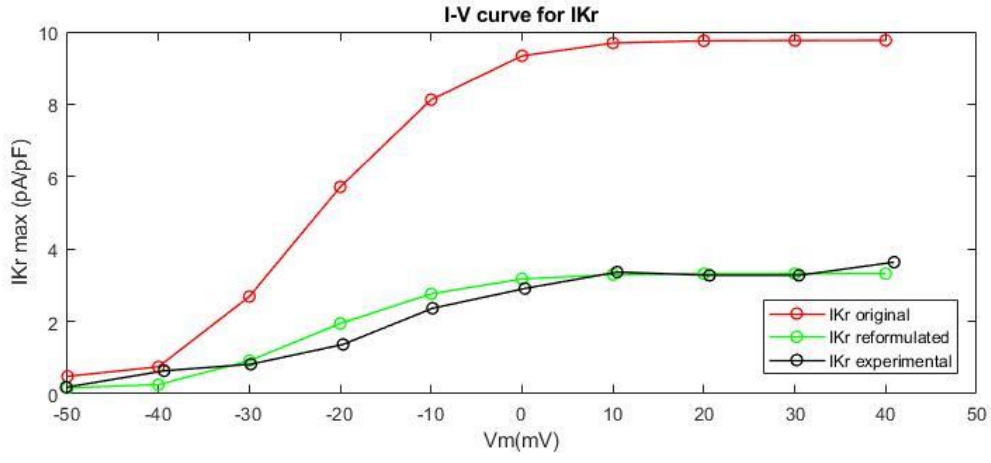

Figure 22: I-V curve for I_{Kr}. Source: Own elaboration.

I_{Kr} is an outward current defined with two gates: P_a, an activation one, and P_i an inactivation one. The equations describing I_{Kr} behaviour in this model are taken from the preliminary AVN model and the modifications are included:

$$I_{Kr} = g_{Kr} * P_a * P_i * (V - E_K) \quad (5\text{-}36)$$

$$P_a = (1 - F_{Kr}) * P_{af} + F_{Kr} * P_{as} \quad (5\text{-}37)$$

$$P_{af_{inf}} = \frac{1}{1 + e^{-\frac{(V+23)}{6.5}}} \quad (5\text{-}38)$$

$$\tau_{af} = \frac{0.84655354}{0.0372 * e^{\frac{V}{15.9}} + 0.00096 * e^{-\frac{V}{22.5}}} \quad (5\text{-}39)$$

$$P_{as_{inf}} = P_{af_{inf}} \quad (5\text{-}40)$$

$$\tau_{as} = \frac{0.84655354}{0.0042 * e^{\frac{V}{17}} + 0.00015 * e^{-\frac{V}{21.6}}} \quad (5\text{-}41)$$

$$P_{i_{inf}} = \frac{1}{1 + e^{\frac{V+15}{6.5}}} \quad (5\text{-}42)$$

$$\tau_i = 2 \quad (5\text{-}43)$$

where F_{Kr} is the fraction for the activation gate and g_{Kr} is the conductance for I_{Kr} expressed in nS/pF.

However, the introduction of I_{Kr} reformulation did not allow the cell to repolarize, see in the subchapter *Final model* for further information.

I_{Ks}

There was not available experimental data for reformulating I_{Ks}. Therefore, the equations which described its behaviour were taken from the preliminary work for AVN model without modification. This current is an outward one with unique activation gate, xs.

$$I_{Ks} = g_{Ks} * xs^2 * (V - E_{Ks}) \quad (5\text{-}44)$$

$$xs_{inf} = \frac{\alpha_{xs}}{\alpha_{xs} + \beta_{xs}} \quad (5\text{-}45)$$

$$\tau_{xs} = \frac{1}{\alpha_{xs} + \beta_{xs}} \quad (5\text{-}46)$$

$$\alpha_{xs} = \frac{0.014}{1 + e^{-\frac{V-40}{9}}} \quad (5\text{-}47)$$

$$\beta_{xs} = 0.001 * e^{-(\frac{V}{45})} \quad (5\text{-}48)$$

where g_{Ks} is the conductance for I_{Ks} expressed in nS/pF.

I_{K1}

No reformulation was done in I_{K1} taking its formulation from the preliminary AVN model.

$$I_{K1} = g_{K1} * \frac{V - E_K}{1 + e^{0.07*(V+80)}} \quad (5\text{-}49)$$

where g_{K1} is the conductance for I_{K1} expressed in nS/pF.

I_{to} and I_{sus}

No reformulation was done for I_{sus}, for I_{to} was considered a simulated Voltage-Clamp protocol where voltage holding was -70 mV and went from -40 mV to +50 mV by 10 mV step, shown in Figure 23A, to obtain the fitting of the I-V curve, shown in Figure 24. The only modification done was a conductance increase by multiplying it per 2.74.

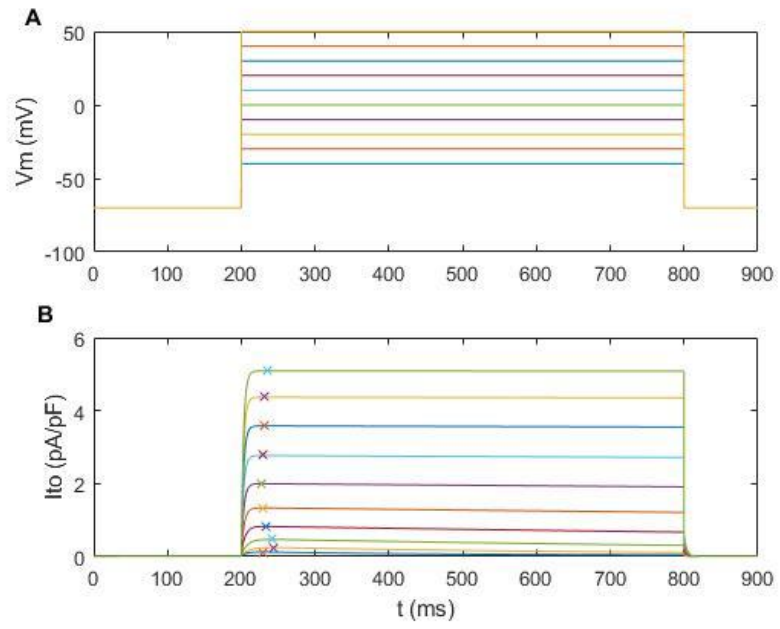

Figure 23: (A): Voltage-Clamp protocol for I_{to}. (B): I_{to} for mouse AVN single cell and maximal current values (x). Source: Own elaboration.

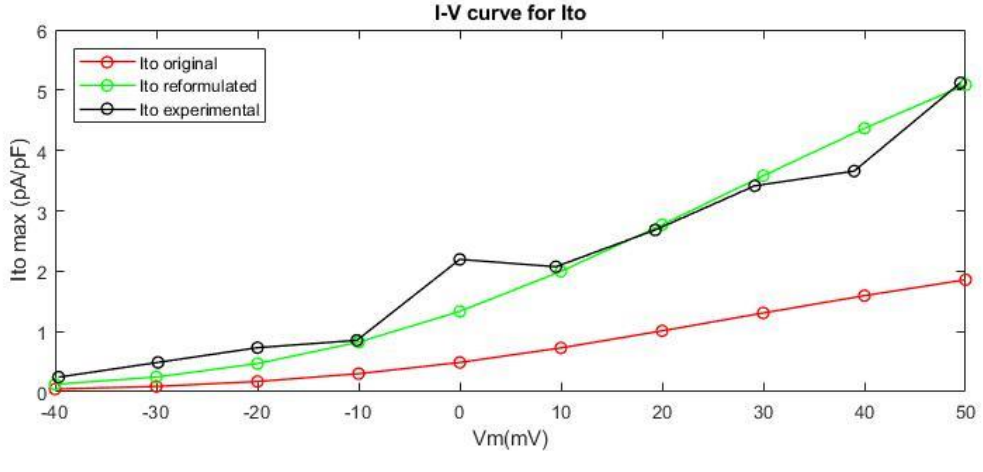

Figure 24: I-V curve for I_{to}. Source: Own elaboration.

The equations description are taken from the previous work for AVN model and the conductance increase is considered. While I_{to} is defined with both activation, r, and inactivation gates, q, I_{sus} only takes into account the activation one, r.

$$I_{to} = g_{to} * q * r * (V - E_K) \quad (5\text{-}50)$$

$$I_{sus} = g_{sus} * r * (V - E_K) \quad (5\text{-}51)$$

$$q_{inf} = \frac{1}{1 + e^{\frac{V+59.37}{13.1}}} \quad (5\text{-}52)$$

$$r_{inf} = \frac{1}{1 + e^{\frac{-(V-10.93)}{19.7}}} \quad (5\text{-}53)$$

$$\tau_q = 10.1 + \frac{65.17}{0.57 * e^{-0.08*(V+49)} + 0.000024 * e^{0.1*(V+50.93)}} \quad (5\text{-}54)$$

$$\tau_r = 2.98 + \frac{15.59}{1.037 * e^{0.09*(V+30.61)} + 0.369 * e^{-0.12*(V+23.84)}} \quad (5\text{-}55)$$

where g_{to} is the conductance for I_{to}, and g_{sus} is the conductance for I_{sus} both expressed in nS/pF.

I_{st}

I_{st} was not modified. Its kinetics are modelled by the equations taken from the preliminary AVN model where two gates are considered, d_s and f_S.

$$I_{st} = g_{st} * d_s * f_s * (V - E_{st}) \quad (5\text{-}56)$$

$$d_{s_{inf}} = \frac{\alpha_{d_s}}{\alpha_{d_s} + \beta_{d_s}} \quad (5\text{-}57)$$

$$\tau_{d_s} = \frac{1}{\alpha_{d_s} + \beta_{d_s}} \quad (5\text{-}58)$$

$$\alpha_{d_s} = \frac{1}{0.15 * e^{-\frac{V}{11}} + 0.2 * e^{-\frac{V}{700}}} \quad (5\text{-}59)$$

$$\beta_{d_s} = \frac{1}{16 * e^{\frac{V}{8}} + 15 * e^{\frac{V}{50}}} \quad (5\text{-}60)$$

$$f_{S_{inf}} = \frac{\alpha_{f_s}}{\alpha_{f_s} + \beta_{f_s}} \quad (5\text{-}61)$$

$$\tau_{f_s} = \frac{1}{\alpha_{f_s} + \beta_{f_s}} \quad (5\text{-}62)$$

$$\alpha_{f_s} = \frac{1}{3100 * e^{-\frac{V}{13}} + 700 * e^{-\frac{V}{70}}} \quad (5\text{-}63)$$

$$\beta_{f_s} = \frac{1}{95 * e^{-\frac{V}{10}} + 50 * e^{\frac{V}{700}}} + \frac{0.000229}{1 + e^{-\frac{V}{5}}} \quad (5\text{-}64)$$

where g_{st} is the conductance for I_{st} expressed in nS/pF.

I_{KACh}

I_{KACh} was taken from the SAN model and although its original contribution was null as it was introduced by changing its conductance different from 0.

$$I_{KACh} = g_{KACh}(K_i - (K_o * e^{-\frac{VF}{RT}}) \quad (5\text{-}65)$$

where $g_{KACh}$is defined such as $0.001\frac{nS}{pF*mM} * K_o^{0.41}\ mM$.

I_{SK}

I_{SK} was introduced in the presented model from JSim model and this current did not suffer any modification. This current behaviour is modelled by the existence of two gates called m_{cak}which depend on calcium concentrations.

$$I_{SK} = g_{SK} * m_{cak}^2 * (V - E_K) \quad (5\text{-}66)$$

$$m_{cak_{inf}} = \frac{Car}{1 + Car} \quad (5\text{-}67)$$

$$\tau_{cak} = \frac{0.001}{beta_k * (1 + Car)} \quad (5\text{-}68)$$

$$Ca_r = \left(\frac{Ca_{sub}}{Ca_c}\right)^{n_{SK}} \quad (5\text{-}69)$$

where g_{SK} is the conductance for I_{SK} expressed in nS/pF.

5.3.3 Calcium currents

Comparing calcium currents with experimental data was also an important point because of its importance on calcium handling. As in the reference there is no evidence for L-type 1.2 calcium current, although it is formulated in the model, its contribution remains 0 being its conductance 0.

$I_{CaL(1.3)}$

L-type 1.3 calcium current was compared with experimental data by using its I-V curve, shown in Figure 26, from a Voltage-Clamp protocol where voltage holding is -55 mV and different voltage test indicated in the Figure 25A. The conductance of this current has been reduced by being multiplied per 0.345 to fit the current peaks computed. Moreover, the reversal potential for calcium has also been changed to the one the data have shown, 34.5 mV, as an important difference between both, the experimental and the calculated one, has been noticed. In the previous model, this potential was calculated using the Nernst equation based on intracellular and extracellular calcium. Nevertheless, it does not seem to be reliable due to the difficulties in calculating calcium concentrations with calcium handling introduction.

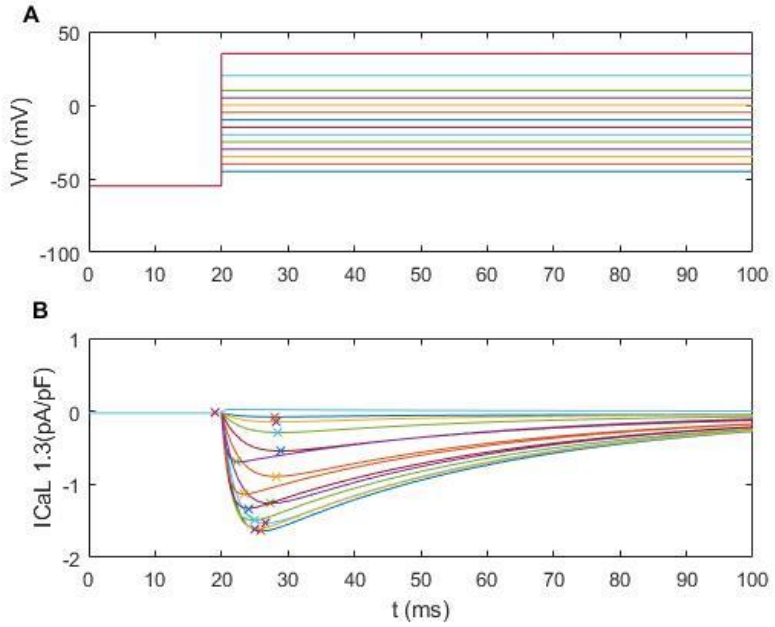

Figure 25: (A): Voltage-Clamp protocol for $I_{CaL(1.3)}$. (B): $I_{CaL(1.3)}$ for mouse AVN single cell and maximal current values (x). Source: Own elaboration.

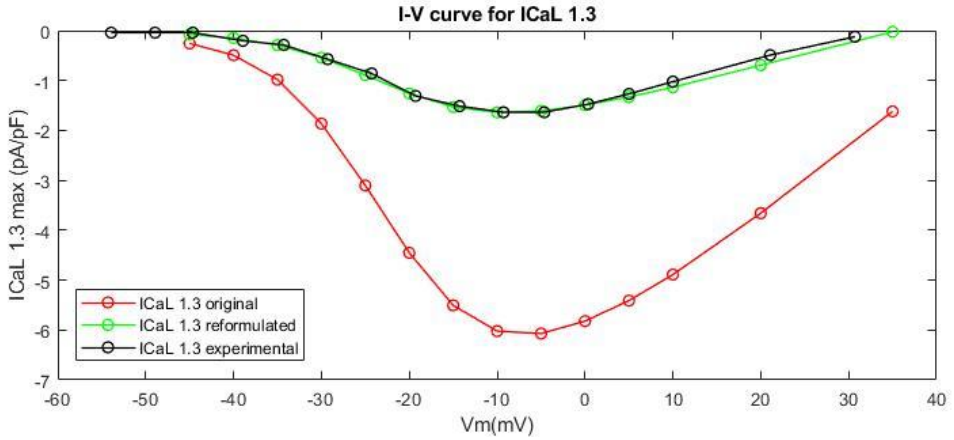

Figure 26: I-V curve for $I_{CaL(1.3)}$. Source: Own elaboration.

Its behaviour is represented by the following equations which are taken from the preliminary work for AVN model where there were considered two gates: an activation, d_D and inactivation, f_D, one.

$$I_{CaD} = g_{CaD} * \left(f_D * d_D + \frac{0.006}{1 + e^{-\frac{V+14.1}{6}}} \right) * (V - E_{Ca}) \quad (5\text{-}70)$$

$$d_{D_{inf}} = \frac{1}{1 + e^{-\frac{V+22}{6.3}}} \quad (5\text{-}71)$$

$$\tau_{d_D} = \frac{1}{\alpha_{d_D} + \beta_{d_D}} \quad (5\text{-}72)$$

$$\alpha_{d_D} = -\frac{0.01419 * (V + 35)}{e^{-\frac{V+35}{2.5}} - 1} - \frac{0.04245 * V}{e^{-0.208*V} - 1} \quad (5\text{-}73)$$

$$\beta_{d_D} = \frac{0.00571 * (V - 5)}{e^{0.4*(V-5)} - 1} \quad (5\text{-}74)$$

$$f_{D_{inf}} = \frac{1}{1 + e^{\frac{V+48}{5.4}}} \quad (5\text{-}75)$$

$$\tau_{f_D} = \frac{1}{\alpha_{f_D} + \beta_{f_D}} \quad (5\text{-}76)$$

$$\alpha_{f_D} = \frac{0.00312 * (V + 28)}{e^{\frac{V+28}{4}} - 1} \quad (5\text{-}77)$$

$$\beta_{f_D} = \frac{0.025}{1 + e^{-\frac{V+28}{4}}} \quad (5\text{-}78)$$

where g_{CaD} is the conductance of I_{CaD} expressed in nS/pF.

I_{CaT}

The experimental data used to reformulated T-type calcium current is an I-V curve, shown in Figure 28, where both, L-type 1.3 and T-type calcium current are considered. Therefore, a reformulated L-type 1.3 calcium current was introduced in order to be consistent with the result. The Voltage-Clamp protocol presented a voltage holding of -55 mV and different voltage test indicated in Figure 27A.

It was needed to consider a decreased in T-type calcium conductance, it was multiplied per 0.83, and the reversal potential has been established as the same in I_{CaL} to fit the current peaks computed. Moreover, a reduction of 6 mV in the half voltage activation has been implemented which turns it in 39 mV.

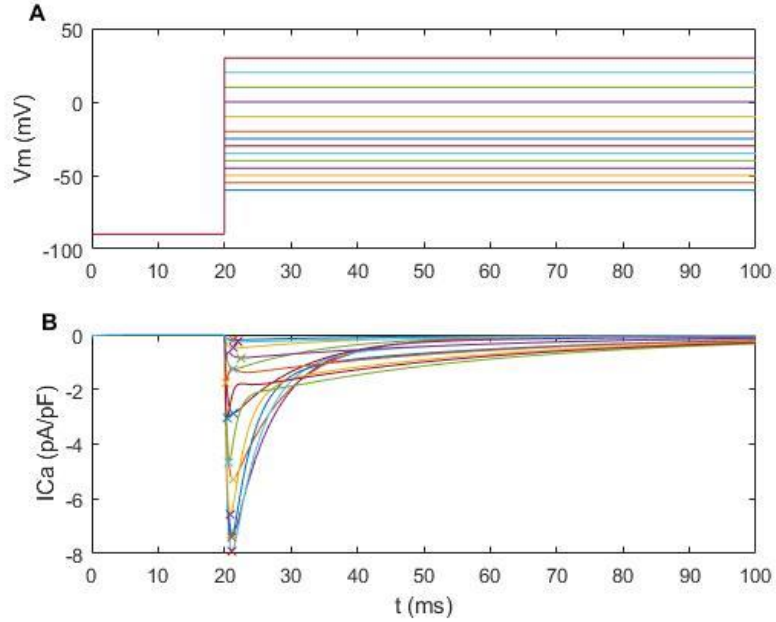

Figure 27: (A): Voltage-Clamp protocol for I_{Ca}. (B): I_{Ca} for mouse AVN single cell and maximal current values (x). Source: Own elaboration.

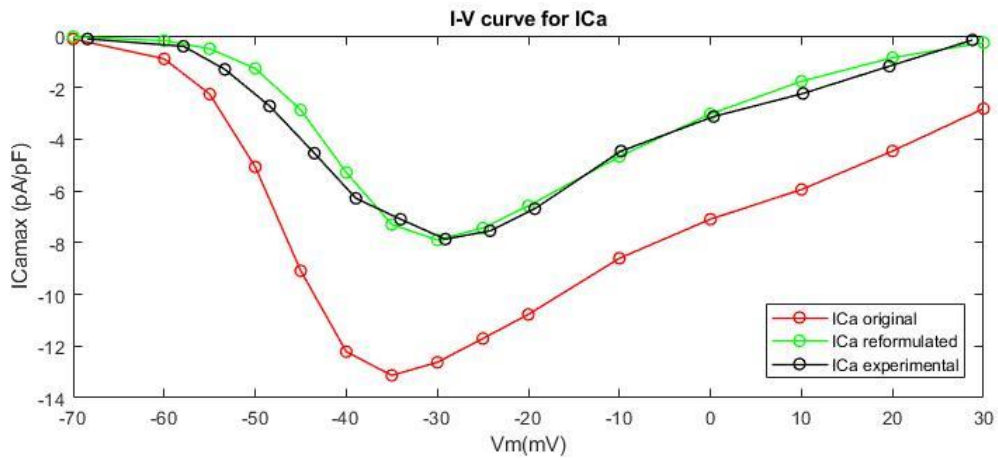

Figure 28: I-V curve for I_{Ca} (I_{CaT}+$I_{CaL(1.3)}$). Source: Own elaboration.

The equations modelling this current behaviour were taken from the previous work and the modifications were considered. It was also considered two gates: activation, d_T and inactivation, f_T, one.

$$I_{CaT} = g_{CaT} * d_T * f_T * (V - E_{CaT}) \quad (5\text{-}79)$$

$$d_{T_{inf}} = \frac{1}{1 + e^{-\frac{V+39}{4.64}}} \quad (5\text{-}80)$$

$$\tau_{d_T} = \frac{1}{\alpha_{d_T} + \beta_{d_T}} \quad (5\text{-}81)$$

$$\alpha_{d_T} = 1.068 * e^{\frac{V+26.3}{30}} \quad (5\text{-}82)$$

$$\beta_{d_T} = 1.068 * e^{-\frac{V+26.3}{30}} \quad (5\text{-}83)$$

$$f_{T_{inf}} = \frac{1}{1 + e^{\frac{V+71}{3.4}}} \quad (5\text{-}84)$$

$$\tau_{f_T} = \frac{1}{\alpha_{f_T} + \beta_{f_T}} \quad (5\text{-}85)$$

$$\alpha_{f_T} = 0.0153 * e^{-\frac{V+71.7}{83.3}} \quad (5\text{-}86)$$

$$\beta_{f_T} = 0.015 * e^{V+\frac{71.1}{15.38}} \quad (5\text{-}87)$$

where g_{CaT} is the conductance of I_{CaT} expressed in nS/pF.

5.3.4 I_f current

The current formulation has been changed to Karche's one [4] because its I-V curve fitted much better with the experimental data considered, shown in Figure 30. Nevertheless, some modifications have been set up in the parameters. The half-activation voltage has been reduced to -97 mV [5] [7], the conductance has been20% reduced and the slope factor has been increased from 16.3 to 20. Furthermore, although Karche's formulation presented different contributions from sodium and potassium currents to I_f, it has been considered the same proportion for both as there is no evidence for AVN not to equally compute these currents.

The fitting has been done by the comparison between the I-V curve obtained by simulation and the experimental one. It has been implemented a Voltage-Clamp protocol where the voltage holding is -30 mV and the voltage test goes from -130 mV to -70 mV in steps of 10 mV and also 0 mV has been evaluated, shown in Figure 29A.

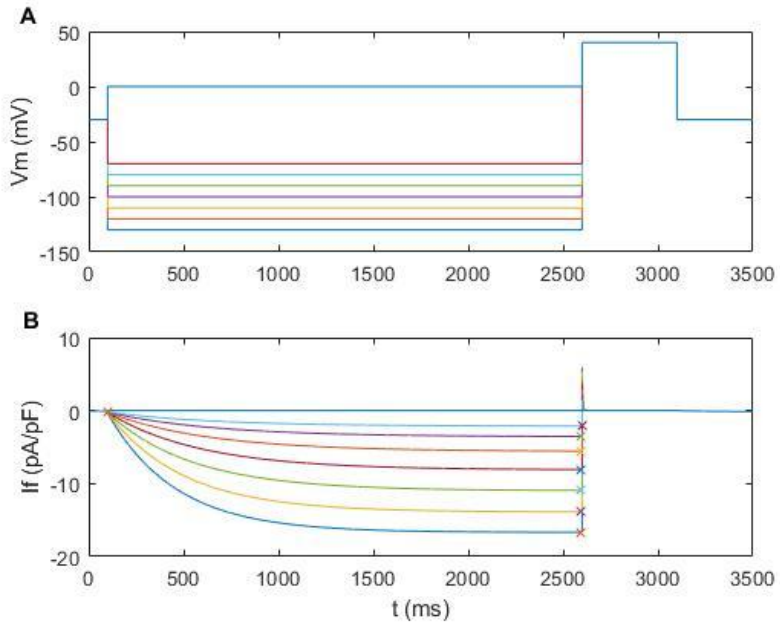

Figure 29: (A): Voltage-Clamp protocol for I_f. (B): I_f for mouse AVN single cell and maximal current values (x). Source: Own elaboration.

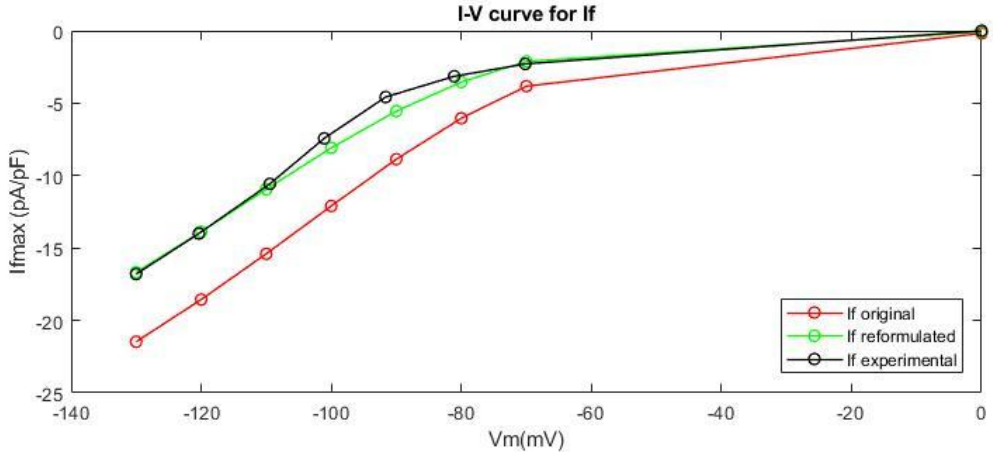

Figure 30: I-V curve for I_f. Source: Own elaboration.

Moreover, also time constant (τ_P) was modified from the Kharche's formulation to obtain the Gaussian peak at -80 mV and a a slower kinetics of its activation in the diastolic phase. It was used a graphic of its voltage dependence, from -300 to 80 mV and compared to τ_P described in the preliminary AVN model in order to fit Kharche's τ_P, shown in Figure 31.

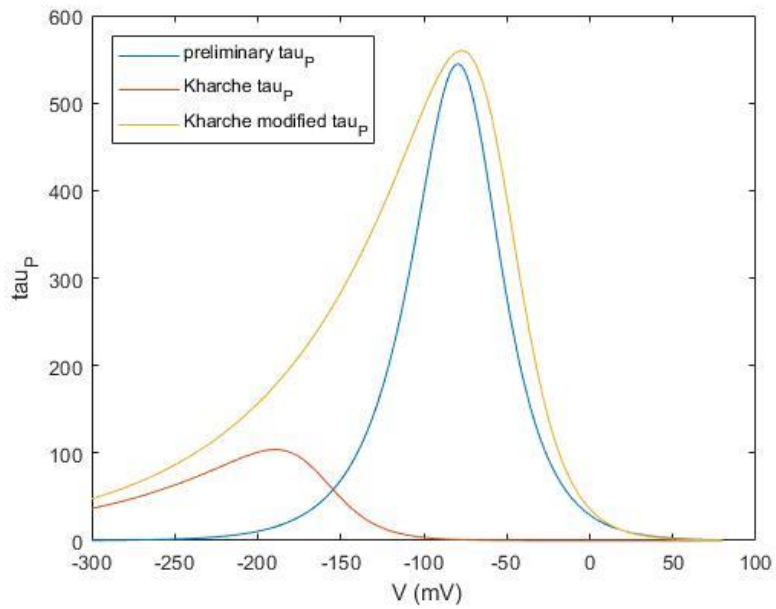

Figure 31: τ_P voltage dependence graphic. Source: Own elaboration.

In I_f definition appears just one inactivation gate, P. Therefore, the implemented equations for I_f are:

$$If = i_{f_{Na}} + i_{f_K} \quad (5\text{-}88)$$

$$i_{f_{Na}} = 0.3833 * gh * P * (V - E_K) \quad (5\text{-}89)$$

$$i_{f_K} = 0.3833 * gh * P * (V - E_{Na}) \quad (5\text{-}90)$$

$$P_{inf} = \frac{1}{1 + e^{\frac{V+V_f}{vslope}}} \quad (5\text{-}91)$$

$$\tau_P = \frac{1.505}{e^{-0.0119(V+590.3)} + e^{\frac{V-55}{17.2}}} \quad (5\text{-}92)$$

where gh is the conductance of $i_{f_{Na}}$ and i_{f_K} expressed in nS/pF.

5.3.5 Background currents

I_{bNa}, I_{bCa} and I_{bK} were not modified and their equations were taken from the previous model for AVN.

$$I_{bNa} = g_{bNa} * (V - E_{Na}) \quad (5\text{-}93)$$

$$I_{bCa} = g_{bCa} * (V - E_{Ca}) \quad (5\text{-}94)$$

$$I_{bK} = g_{bK} * (V - E_K) \quad (5\text{-}95)$$

where g_{bNa}, g_{bCa} and g_{bK} are the conductances for I_{bNa}, I_{bCa} and I_{bK} expressed in nS/pF and E_{Na}, E_{Ca} and E_K are the reversal potential for Na^+, Ca^{+2} and K^+ expressed in mV.

5.3.6 Sodium-Calcium exchanger

Although no reformulation was done in I_{NaCa} based on experimental data, its maximal value was 10% reduced due to the calcium handling introduction and calcium intracellular concentration changing.

$$I_{NaCa} = \frac{1}{C_m}\frac{1000}{10} * K_{NaCa} * \frac{Nai^3 * Cao * e^{0.03743*V*\gamma_{NaCa}} - Nao^3 * Cai * e^{0.0374*V*(\gamma_{NaCa}-1)}}{1 + d_{NaCa} * (Cai * Nao^3 + Cao * Nai^3)} \quad (5\text{-}96)$$

where K_{NaCa} is the maximum value for this I_{NaCa} expressed in pA.

5.3.7 Sodium-Potassium pump

Its formulation was taken from the preliminary AVN model without any modification.

$$I_{NaK} = \frac{1}{C_m} * I_{NaK_{max}} * \left(\frac{Nai}{K_{m_{Na}} + Nai}\right)^3 * \left(\frac{Ko}{K_{m_K} + Ko}\right)^2 * \frac{1.6}{1.5 + e^{-\frac{V+60}{40}}} \quad (5\text{-}97)$$

where $I_{NaK_{max}}$ is the maximum value for I_{NaK} expressed in pA, $K_{m_{Na}}$ and K_{m_K} are the half-maximum dependence concentrations of Na and K expressed in mM.

5.4 Problematic currents reformulated introduction and final model presented

All exposed modifications were introduced in the preliminary AVN model and its resulting consistency was analysed. There were two current reformulations the model could not work with.

On one hand, I_{Nar} reformulation made the cell stop beating after 800 ms simulation, shown in Figure 32. This current is the principal responsible for generating the AP upstroke and not enough I_{Nar} would not make possible depolarizing the cell. In this reformulation case, the conductance has been multiplied per 0.034 in order to standardize the activation gate definition. This reduction is not consistent with the model presented. In Figure 32, it is shown how the current decreases, as well as the V_{max}, until finally the cell is not able to depolarize and stops beating. Therefore, it has been established to use the previous I_{Nar} formulation and await for more experimental data.

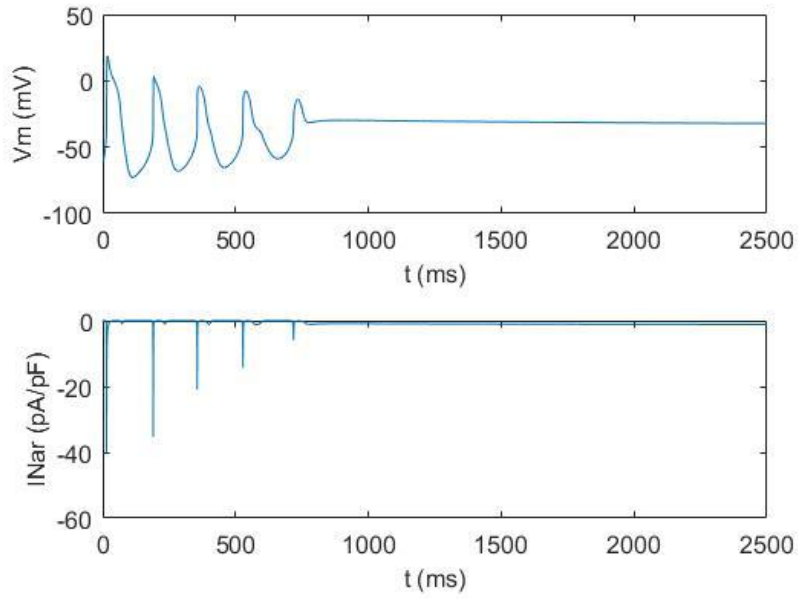

Figure 32: (A): Mouse AP AVN single-cell with I_{Nar} reformulation included (B): I_{Nar} time course. Source: Own elaboration.

On the other hand, I_{Kr} reformulation also needed a high reduction of its conductance. As this current is the one mostly responsible for cell repolarization in phase 3, an important reduction of its conductance could lead incomplete cell repolarization. In this case, it was needed to multiply the conductance per 0.34 in order to fit I-V curve with experimental data. Nevertheless, the presented model only allowed a conductance multiplied per 0.8 to be able to repolarize the cell. The reduction required was far greater than the model could withstand. It is shown in Figure 33 that the cell is not able to repolarize in the first AP displayed because of the I_{Kr} reduction. Therefore, it was decided not to include this modification in the presented model and await for more experimental data.

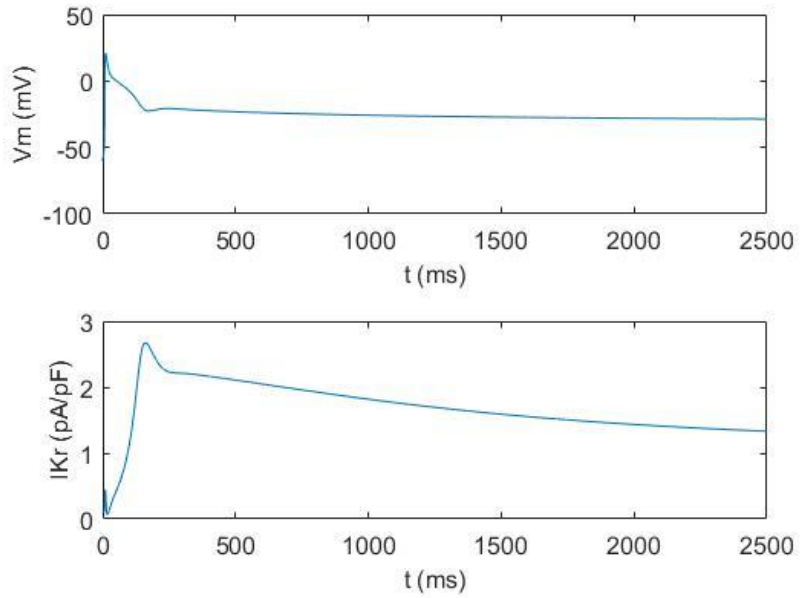

Figure 33: (A): Mouse AP AVN single-cell with I_{Kr} reformulation included (B): I_{Kr} time course.. Source: Own elaboration.

Summarizing, all the modifications exposed in Table 4 were included apart from I_{Nar} and I_{Kr} reformulations which have been formulated as they were in the preliminary AVN model. Therefore, the paramaters values have not been changed and the activation gate for I_{Nar} is:

$$m_{inf_{Nar}} = \frac{1}{1 + e^{\frac{V+V_{act_r}}{-sNa_r}}} \qquad (5\text{-}98)$$

Table 4: Summary of included currents.

Current	Taken from	Reformulation	
		Original	Reformulated
$\boldsymbol{I_{Nar}}$	AVN preliminary model	g_{Na_r} $V_{act_{Nar}} = 43\ mV$ $sNa_r = 7$ $m_{inf_r} = \left(\frac{1}{1 + e^{\frac{V+V_{act_r}}{-sNa_r}}}\right)^{1/3}$	$0.034 * g_{Na_r}$ $V_{act_{Nar}} = 39\ mV$ $sNa_r = 3$ $m_{inf_r} = \frac{1}{1 + e^{\frac{V+V_{act_r}}{-sNa_r}}}$
$\boldsymbol{I_{Nas}}$	AVN preliminary model	g_{Na_s} $V_{act_{Nas}} = 31\ mV$ $sNa_s = 4.4$ $m_{inf_s} = \left(\frac{1}{1 + e^{\frac{V+V_{act_s}}{-sNa_s}}}\right)^{1/3}$	$0.066 * g_{Na_s}$ $V_{act_{Nas}} = 36\ mV$ $sNa_s = 4$ $m_{inf_s} = \frac{1}{1 + e^{\frac{V+V_{act_s}}{-sNa_s}}}$

$I_{CaL\,(1.3)}$	AVN preliminary model	g_{CaD} $E_{CaD} = 46.4\ mV$	$0.345 * g_{CaD}$ $E_{CaD} = 34.5\ mV$
$I_{CaL\,(1.2)}$	AVN preliminary model	– – – –	– – – –
I_{CaT}	AVN preliminary model	g_{CaT} $E_{CaT} = 45\ mV$ $V_{act_{CaT}} = 39\ mV$	$0.83 * g_{CaT}$ $E_{CaT} = E_{CaD}$ $V_{act_{CaT}} = 45\ mV$
I_{Kr}	AVN preliminary model	g_{Kr}	$0.34 * g_{Kr}$
I_{Ks}	AVN preliminary model	– – – –	– – – –
I_{K1}	AVN preliminary model	– – – –	– – – –
I_{to}	AVN preliminary model	g_{to}	$2.74 * g_{to}$
I_{sus}	AVN preliminary model	– – – –	– – – –
I_f	Kharche et al (2011)	g_h $V_{act_f} = -106.8\ mV$ $sf = 16.3$ $\tau_P = \frac{1.505}{e^{-0.011(V+590.3)} + e^{\frac{V+85.1}{17.2}}}$	g_h $V_{act_f} = -97\ mV$ $sf = 20$ $\tau_P = \frac{1.505}{e^{-0.0119(V+590.3)} + e^{\frac{V-55}{17.2}}}$
I_{KACh}	SAN JSim model	$g_{KACh} = 0$	$g_{KACh} = 0.001 * K_o^{0.41}$
I_{st}	AVN preliminary model	– – – –	– – – –
I_{SK}	SAN JSim model	– – – –	– – – –
I_{NaK}	AVN preliminary model	– – – –	– – – –
I_{NaCa}	AVN preliminary model	K_{NaCa}	$K_{NaCa}/10$
I_{bNa}	AVN preliminary model	– – – –	– – – –
I_{bK}	AVN preliminary model	– – – –	– – – –
I_{bCa}	AVN preliminary model	– – – –	– – – –

CHAPTER 6: **RESULTS AND DISCUSSION**

In this chapter, it will be analysed the AVN action potential obtained from all the modifications previously explained. Firstly, intracellular calcium concentrations will be analysed in order to choose the parameter values which better fix reality. Then, biomarkers exposed in *Methods* will be calculated and compared to AVN experimental data shown in Table 2 and Table 3. Finally, it will be studied the effect of I_f in this model.

6.1 Intracellular calcium concentration analysis

Intracellular calcium concentrations obtained after the introduction of calcium handling equations to the model without any changes are shown in Figure 34.

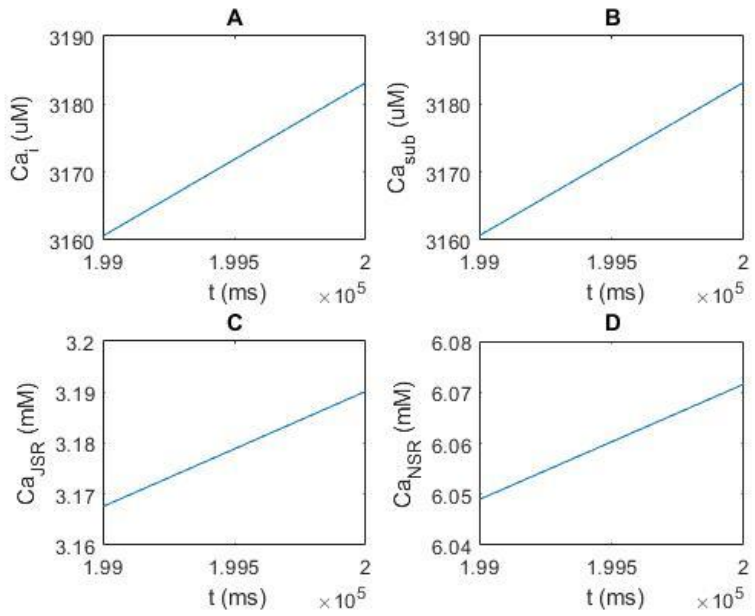

Figure 34: Time course of (A) intracellular calcium (B) subspace calcium (C) JSR calcium (D) NSR calcium with no changes in calcium handling equations. Source: Own elaboration.

It can be observed in Figure 34 a calcium accumulation. This behaviour was related to an error in balance intracellular calcium equation which was copied from JSim model and needed to correct it. Specifically, the uptake flux contribution was normalized by the JSR when it must be normalized by NSR. Once, this error was corrected the results obtained are shown in Figures 35 and 36.

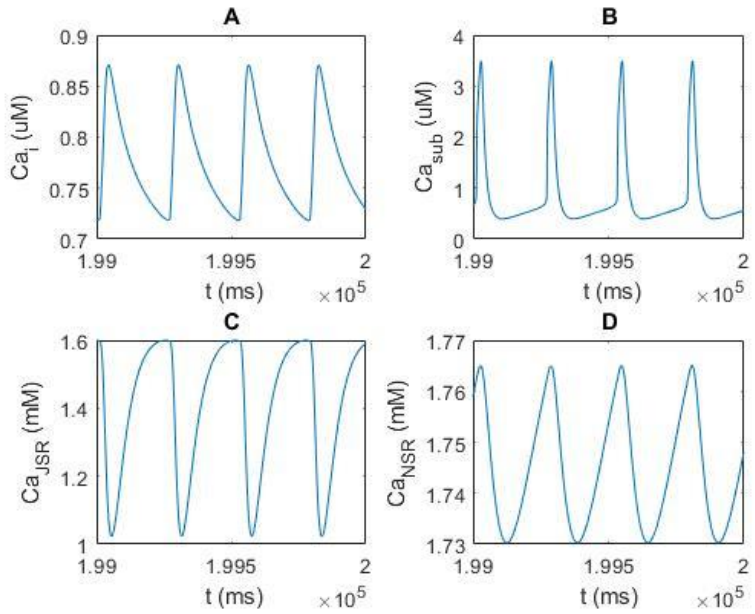

Figure 35: Last seconds of long simulation of the time course (A) intracellular calcium (B) subspace calcium (C) JSR calcium (D) NSR calcium with the error corrected. Source: Own elaboration.

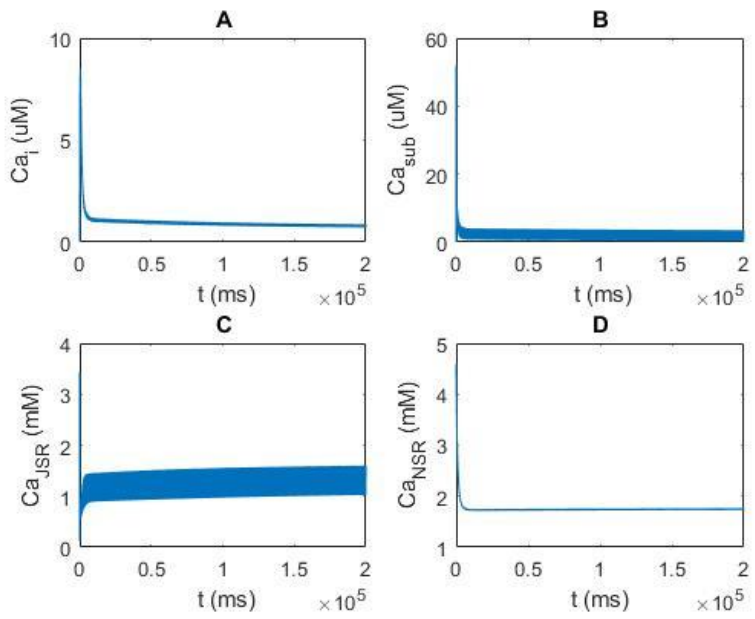

Figure 36: Time course of (A) intracellular calcium (B) subspace calcium (C) JSR calcium (D) NSR calcium with the error corrected. Source: Own elaboration.

Despite not having experimental data to take into account when analysing calcium concentrations, it is known that $[Ca^{+2}]_i$ physiological condition needs to be less than $1\mu M$. Figure 35A shows that this condition is fulfilled and $[Ca^{+2}]_{sub}$ is also in μM range. Otherwise, $[Ca^{+2}]_{JSR}$ and $[Ca^{+2}]_{NSR}$ are considerably higher as its oscillation range is in mM. Figure 36 shows how calcium concentration gets steady-state after 5 seconds simulation.

Some tests were run in which some parameter changes were done in order to study which combination will fit better in the model. The first test was related to a % change in the subspace volume. The one defined in the calcium handling equations, 0.1% of the total cell volume, did not

correspond to the one presented in Kharche's results, 1.1% of the total cell volume, while the other volumes described did. The results are shown in Figure 37.

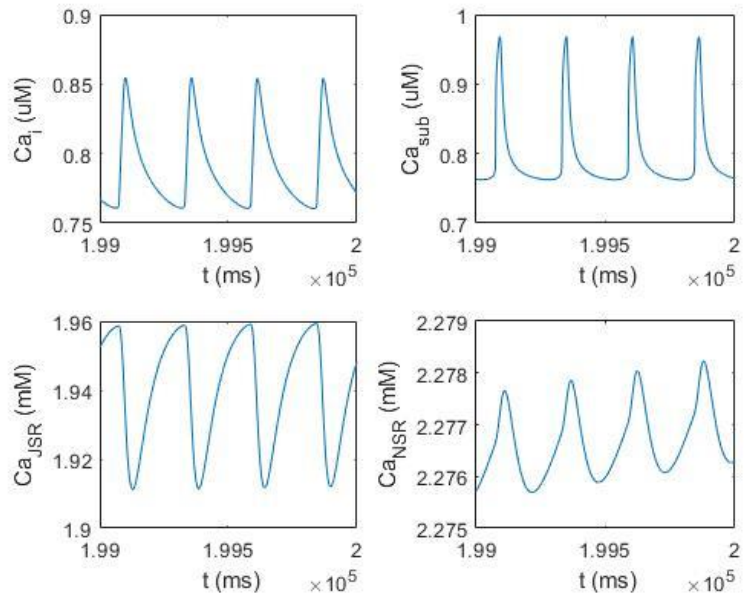

Figure 37: Last seconds of long simulation of the time course (A) intracellular calcium (B) subspace calcium (C) JSR calcium (D) NSR calcium with % subspace volume changed. Source: Own elaboration.

Figure 37 shows that the most significant change is found in the reduction of subspace calcium concentration, which makes sense as this compartment volume has been reduced. Otherwise, the peaks of $[Ca^{+2}]_{JSR}$ and $[Ca^{+2}]_{NSR}$ have slightly increased, but their oscillation range decreased.

Using the % subspace volume defined in JSim model, 0.1%, other tests were done by changing ks, release rate parameter, and K_{up}, half maximal $[Ca^{+2}]_i$ of Ca^{+2} uptake by j_{up} in the NSR,values. Firstly, ks was divided by a factor of 10 and $[Ca^{+2}]_{JSR}$ and $[Ca^{+2}]_{NSR}$ increase their peak, as shown in Figure 38 (blue lines). However, an increase by a factor of 10 in ks makes $[Ca^{+2}]_{sub}$ peak increase, also shown in Figure 38 (red lines).

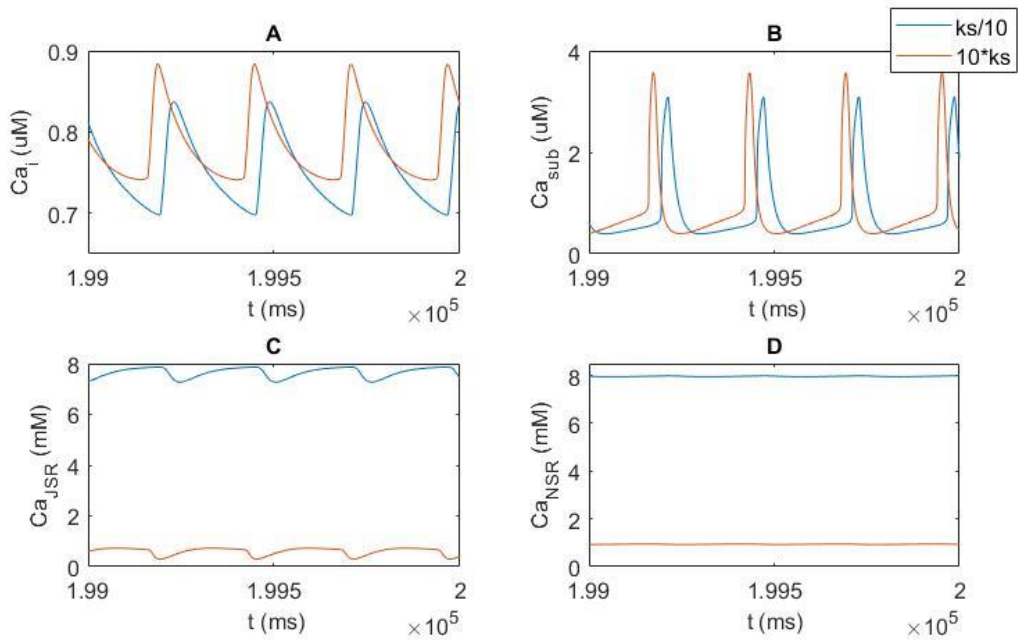

Figure 38: Last seconds of long simulation of the time course (A) intracellular calcium (B) subspace calcium (C) JSR calcium (D) NSR calcium with ks changed. Source: Own elaboration.

Then, K_{up} was reduced by a factor of 10 and $[Ca^{+2}]_{JSR}$ and $[Ca^{+2}]_{NSR}$ increase and $[Ca^{+2}]_{sub}$ shape is not the expected one. It was also increased by a factor of 10 but this test makes the cell stop beating.

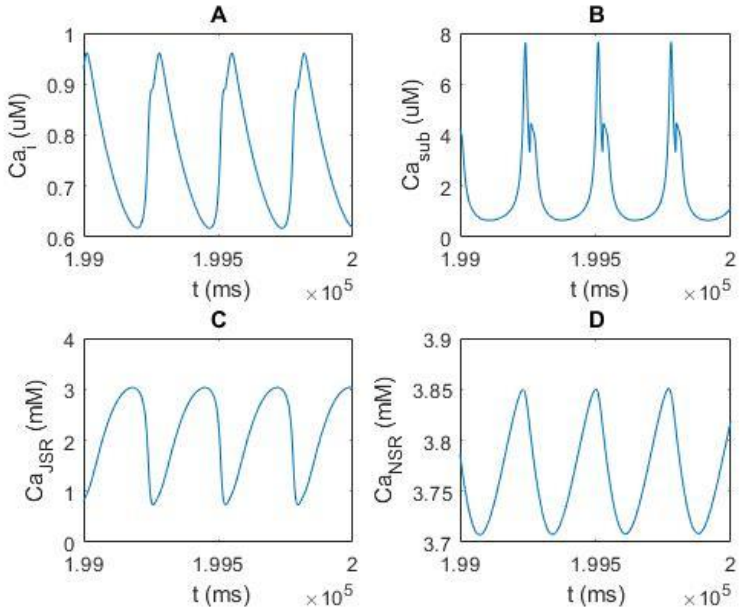

Figure 39: Last seconds of long simulation of the time course (A) intracellular calcium (B) subspace calcium (C) JSR calcium (D) NSR calcium with K_{up} changed. Source: Own elaboration.

It was also tried a combination of changes in both parameters: decreasing by a factor of 10 ks and increasing by a factor of 10 K_{up}. The result is shown in Figure 40 which is really similar to the ones obtained without any change in parameter values, shown in Figure 35.

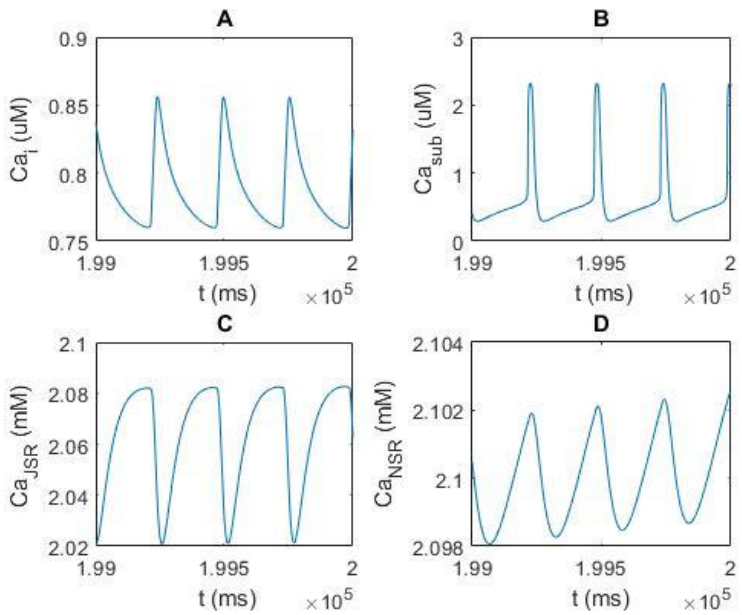

Figure 40: Last seconds of long simulation of the time course (A) intracellular calcium (B) subspace calcium (C) JSR calcium (D) NSR calcium with ks and K_{up} changed. Source: Own elaboration.

Analysing the different possibilities, it was decided to use the values from JSim model as any value parameter changes improved the calcium behaviour.

6.2 Biomarkers analysis

The presented biomarkers, shown in Table 5, have been calculated as a media from all the APs from the steady-state beginning since the end of the simulation, in this case a two hundred seconds simulation. Figure 41 shows the steady-state beginning after 3 seconds of simulation and Figure 42 shows MDP and V_{max} of the action potential modelled.

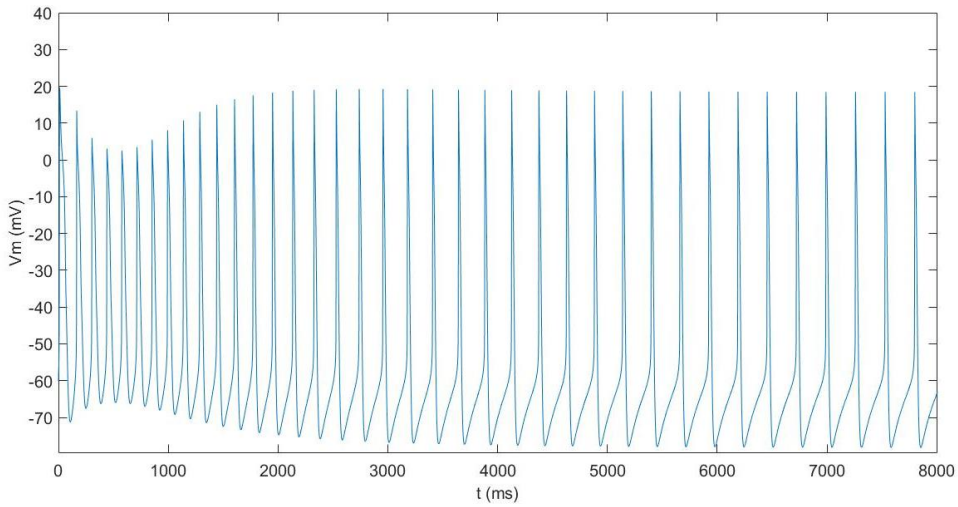

Figure 41: Resulting APs from the presented model. Source: Own elaboration.

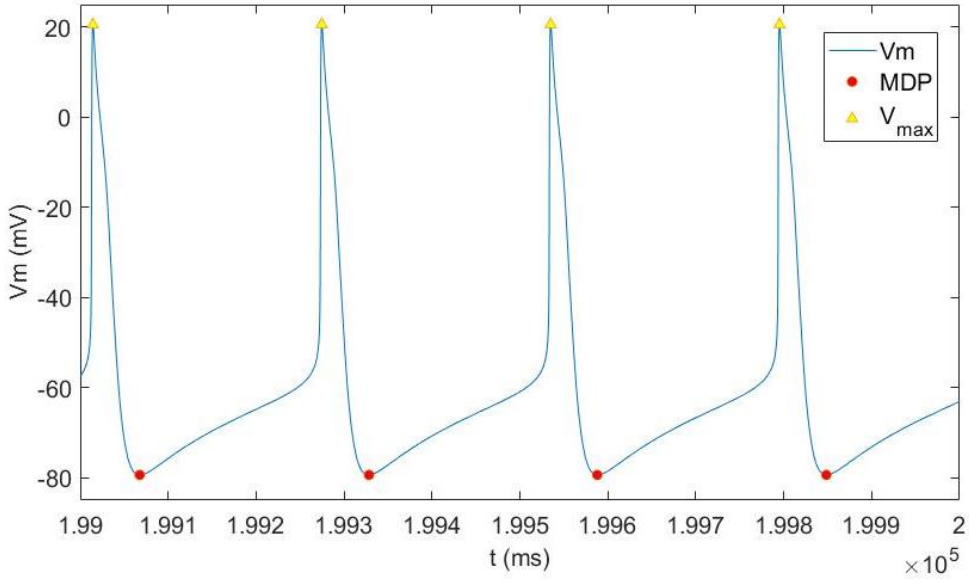

Figure 42: APs from the last seconds of simulation. Source: Own elaboration.

Table 5: Comparison between experimental biomarkers and the ones obtained by the presented model.

	Experimental data		The presented model
$\boldsymbol{Rate(bpm)}$	173 ± 27	$---$	227
$\boldsymbol{MDP(mV)}$	-57 ± 1	-62 ± 1	-79
$\boldsymbol{APA(mV)}$	91 ± 7	76 ± 3	101
$\boldsymbol{APD_{30}(ms)}$	$---$	25 ± 4	22
$\boldsymbol{APD_{50}(ms)}$	$---$	37 ± 6	28
$\boldsymbol{APD_{70}(ms)}$	$---$	60 ± 6	34
$\boldsymbol{APD_{90}(ms)}$	$---$	100 ± 8	43

In Table 5 is shown that APD, at different repolarization voltages, are shorter than the ones exposed in experimental data. On one hand, this fact could be explained by the impossibility of I_{Kr} reformulation together with I_{CaD} and I_{CaT} modification. Calcium currents have been reduced to fit experimental data and although the rapid potassium current was expected to be considerably decreased, this reduction was not included in the model. Both currents, calcium and potassium ones, are responsible for maintaining the plateau during phase 3 and an imbalance between them could directly affect the action potential duration as it is really linked to the plateau lasts. Therefore, it could be thought that the introduction of calcium reformulation but not potassium may have led to an unbalanced outward-inward current on the plateau where I_{Kr} takes the control leading the cell to an early repolarization and reducing APD.

This behaviour is also present in the preliminary AVN model. If I_{Kr} is reduced, the model is unable to repolarize and the reduction of calcium currents makes the APD decrease where APD_{90} is $56.33\ ms$. On the other hand, another reason which could explain this fact is the calcium handling equations introduction as it directly affects calcium currents.

The MDP observed in the presented model, -78,70 mV, is more negative than in experimental data, -57 mV and -62 mV. In the diastolic phase, calcium currents and I_f are the ones taking control of the electrophysiological cell behaviour. Although they have been reformulated according to experimental data, some more experimental information is needed to fit the MDP. These results were already present in both previous models, the preliminary AVN model and JSim model.

APA is not so far away from the experimental data we have. However, this biomarker suggests V_{max} from experimental data is higher than the one obtained in the presented model because its MDP is higher.

6.3 I_f block analysis

The impact of a 50% reduction and block of the 'funny' current has also been analysed. Although this current is not the only one responsible for beating automaticity, it is considered one of the most important for pacemaker activity. Therefore, it is expected that reducing its conductance makes beating frequency slows down. To corroborate this assumption, the rate has been calculated from the cycle length (CL) in three different situations, normal condition, 50% reduction of the current and blocking the current, and shown in Table 6 and Figure 43.

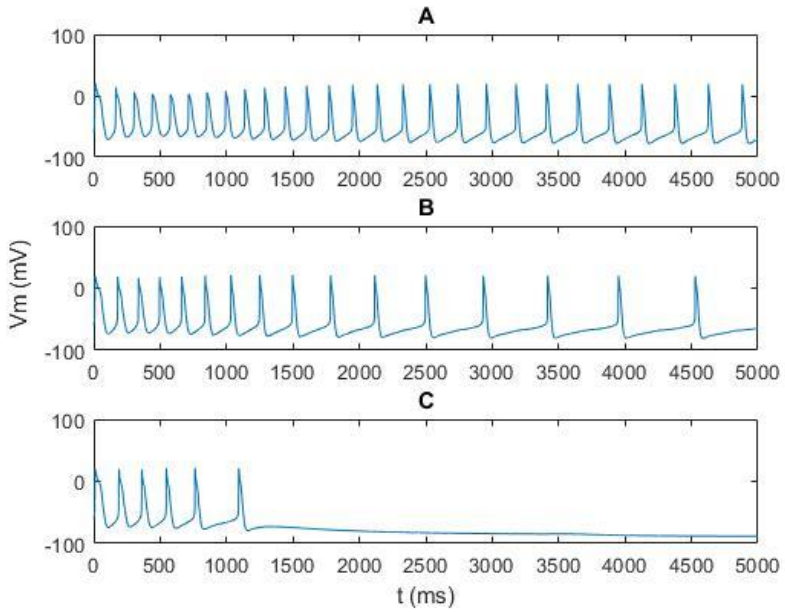

Figure 43: AP with (A) I_f normal condition (B) I_f 50% reduction and (C) I_f block. Source: Own elaboration.

Table 6: Cycle length and rate from different I_f situations.

Condition	CL (ms)	Rate (bpm)
I_f normal condition	262.13	228.90
I_f 50% reduction	608.76	98.56
I_f block	--	--

As expected, an I_f 50% reduction considerably slows down the rate in the presented model. Furthermore, an I_f block does not allow the cell to stabilize and it stops beating.

CHAPTER 7: **LIMITATIONS AND FUTURE WORK**

The presented model is a first approach of a mouse AP single-cell model in which calcium handling has been taken into account.

First, both I_{Nar} and I_{Kr} reformulations need to be included in a future upgrade of the model as their kinetics have been computationally fitted to AVN experimental data. Perhaps other currents with similar participation in the AP have to be reformulated to achieve a consistent model.

By definition, I_{CaL} is an inward current which is present during the depolarization phase. However, it is not considered in the presented model because it was no found in mouse AVN cells [8] of this current when calcium currents were tested. Nevertheless, this experimental finding might be related to the specific AVN region from which cells where taken in tose experiments. Including this current could allow the presence of I_{Nar} into the model. Moreover, introduction of the reformulated, decreased, I_{Kr} should probably be compensated by the increase of other outward currents during the plateau and repolarization phases.

Furthermore, the results for calcium intracellular concentrations had not been compared to any experimental data and some experimental information of these characteristics in the defined cell compartments could be useful in order to fit calcium handling equations. Nevertheless, it is shown in Figure 35 that although $[Ca^{+2}]_i$ and $[Ca^{+2}]_{sub}$ oscillations are within an acceptable range results, $[Ca^{+2}]_{NSR}$ and $[Ca^{+2}]_{JSR}$ are considerably higher than expected and need to be reformulated in order to adjust to a uM oscillation range. Some experimental data in these areas will be useful to fit the equations representing calcium handling.

The principal limitation of this work has been the lack of AVN experimental data. This fact has restricted our work and made the AP obtained quite different from the experimental data we have. As the presented model is not the final version of an AP mouse AVN single-cell model, it is expected that with more experimental data and reformulations introduction these biomarkers fit better.

Finally, a long-term improvement is considering a 2-D mouse AP model to simulate the electrical propagation along with different AVN cells and study different physiological situations.

CHAPTER 8: **CONCLUSIONS**

This work improves an AP mouse AVN single-cell model by the introduction of calcium handling equation to obtain a consistent second generation model.

To accomplish this objective, the calcium handling equations were taken from an AP mouse SAN single-cell model and introduced in the preliminary AVN model which needed to be improved.

Moreover, there were done different currents reformulation based on experimental Voltage-Clamp protocols. I_{Nar}, I_{Nas}, I_f, I_{CaT}, I_{CaD}, I_{to} and I_{Kr} were the currents reformulated and all their modifications were included in the new model version apart from I_{Nar} and I_{Kr} which made the model not working. Additionally, some other modifications were taken into account related to cell capacitance and I_{NaCa} maximum conductance.

Finally, the presented model is not the last version of an AP mouse AVN single-cell model but a first approach where some improvements from the preliminary one have been included: cell compartmentalization, calcium fluxes, dynamic ion intracellular concentrations and calcium buffering. Nevertheless, more experimental data are needed to improve this model including I_{Nar} and I_{Kr} reformulations and fitting in a better way the biomarkers exposed.

CHAPTER 9: **BIBLIOGRAPHY**

[1] J. E. Hall and A. C. Guyton, “Principios generales de la función gastrointestinal: motilidad, control nervioso y circulación sanguínea,” *Tratado Fisiol. médica*, pp. 573–579, 2007.

[2] T. Nikolaidou, O.V. Aslanidi, H. Zhang and I.R. Efimov, “Structure/Function Relationship in the Sinus and Atrioventricular Nodes” *Bone*, vol. 23, no. 1, pp. 1–7, 2012.

[3] M. Delmar and J. Anumonwo, *Electrophysiology Second Edition*. 2009.

[4] S. Kharche, J. Yu, M. Lei, and H. Zhang, “A mathematical model of action potentials of mouse sinoatrial node cells with molecular bases,” *Am. J. Physiol. - Hear. Circ. Physiol.*, vol. 301, no. 3, 2011.

[5] L. Marger *et al.*, “Pacemaker activity and ionic currents in mouse atrioventricular node cells,” *Channels*, vol. 5, no. 3, pp. 241–250, 2011.

[6] P. Mesirca *et al.*, “Cardiac arrhythmia induced by genetic silencing of ‘funny’ (f) channels is rescued by GIRK4 inactivation,” *Nat. Commun.*, vol. 5, no. May, 2014.

[7] M. E. Mangoni and J. Nargeot, “Properties of the hyperpolarization-activated current (If) in isolated mouse sino-atrial cells,” *Cardiovasc. Res.*, vol. 52, no. 1, pp. 51–64, 2001.

[8] M. E. Mangoni *et al.*, “Functional role of L-type Cav1.3 Ca2+ channels in cardiac pacemaker activity,” *Proc. Natl. Acad. Sci. U. S. A.*, vol. 100, no. 9, pp. 5543–5548, 2003.

CHAPTER 10: **APPENDIX**

The code corresponding to the function *main* is the following:

```
clear all
close all

options = odeset('MaxStep',1);

    %% Model Flag
%This flag determines which model is simulatedif mflag=1, SAN is modelled, if it is another number, AVN is modelled
    %mflag=1                          ----> mouse action potential SAN single-cell
    %mflag=other number apart from 1 ----> mouse action potential AVN single-cell

mflag=0;

    %% Initial conditions for the basal cell model

if mflag==1 %SAN
    Y=[];

    Y(1) = -59.08353;  % potential
    Y(2) = 0.09035133; % m activation gate INa
Y(3) = 0.59987707; %h1 inactivation gate INa
Y(4) = 0.13213178; %h2 inactivation gate INa
Y(5) = 0.00165664; % ms activation gate INas
Y(6) = 0.93676454; %h1s inactivation gate INas
Y(7) = 0.16602175; %h2s inactivation gate INas

Y(9)  = 0.00060313339; % d_L activation gate ICaL Cav1_2
Y(10) = 0.99357473; %f_L inactivation gate ICaL Cav1_2

Y(11) = 0.00472538; %d_D activation gate ICaL Cav1_3
Y(12) = 0.9717401; %f_D inactivation gate ICaL Cav1_3

Y(13) = 0.00415744; %d_T activation gate ICaT
Y(14) = 0.61198717; % f_T inactivation gate ICaT

Y(15) = 0.02165677; %P_af activation fast gate Ikr
Y(16) = 0.16201688; %P_as activation slow gate Ikr
Y(17) = 0.85914836; % P_i inactivation gate Ikr

Y(18) = 0.76722397; % q inactivation gate Ito
Y(19) = 0.00491515; % r activation gate Ito and I_sus

Y(20) = 0.12369196; %P hyperpolarisation_activated_current_y_gate

Y(21) = 0.34819037; %d_s sustained_inward_current_d_gate
Y(22) = 0.67467869; %f_s sustained_inward_current_f_gate

Y(23) = 0.0119054; %xs gate slow_delayed_rectifying_potassium_current
```

```
    Y(24) = 0.99979196;%0; %m_cak

    Y(25) = 0.64484881; %R1
    Y(26) = 0.000012240116; %O1
    Y(27) = 0.0000067409369; %I1

    Y(28) = 18.87833; %Nai
    Y(29) = 159.43881; %Ki
    Y(30) = 0.00416387; %Cai
    Y(31) = 0.00102522; %Ca_sub
    Y(32) = 4.5887879; %CaNSR
    Y(33) = 3.431262; %CaJSR

    Y(34) = 0.45367981; %fTC
    Y(35) = 0.93724623; %fMC
    Y(36) = 0.05542706; %fTMM
    Y(37) = 0.6364781; %fCMi
    Y(38) = 0.29785784; %fCMs
    Y(39) = 0.84628533; %fCQ

    Y(40) = 0.27581564; %fCa
else %AVN
    Y=[];

    Y(1) = -60.1; % potential
    Y(2) = 0.135; % m activation gate INa
    Y(3) = 0.03123; %h1 inactivation gate INa
    Y(4) = 1;%4.894; %h2 inactivation gate INa
    Y(5) = 0.135; % ms activation gate INas
    Y(6) = 0.03123; %h1s inactivation gate INas
    Y(7) = 1;%4.894; %h2s inactivation gate INas

    Y(9)  = 0.02248; % d_L activation gate ICaL Cav1_2
    Y(10) = 0.43; %f_L inactivation gate ICaL Cav1_2

    Y(11) = 0.02248; %d_D activation gate ICaL Cav1_3
    Y(12) = 0.531; %f_D inactivation gate ICaL Cav1_3

    Y(13) = 0.02217; %d_T activation gate ICaT
    Y(14) = 0.06274; % f_T inactivation gate ICaT

    Y(15) = 0.002359413; %P_af activation fast gate Ikr
    Y(16) = 0.09102082; %P_as activation slow gate Ikr
    Y(17) = 0.9977152; % P_i inactivation gate Ikr

    Y(18) = 0.06609; % q inactivation gate Ito
    Y(19) = 0.05733; % r activation gate Ito and I_sus

    Y(20) = 0.007645; %P hyperpolarisation_activated_current_y_gate

    Y(21) = 0.0015225; %d_s sustained_inward_current_d_gate
    Y(22) = 0.283; %f_s sustained_inward_current_f_gate

    Y(23) = 0; %xs gate slow_delayed_rectifying_potassium_current

    Y(24) = 0.99979196;%0; %m_cak

    Y(25) = 0.64484881; %R1
    Y(26) = 0.000012240116; %O1
```

```
    Y(27) = 0.0000067409369; %I1

    Y(28) = 18.87833; %Nai
    Y(29) = 159.43881; %Ki
    %Y(30) = 0.00416387; %Cai
    Y(30) = 0.0000326892; %Cai
    %Y(31) = 0.00102522; %Ca_sub
    Y(31) = 0.0000534741; %Ca_sub
    Y(32) = 4.5887879; %CaNSR
    %Y(32) = 0.1038669181; %CaNSR
    Y(33) = 3.431262; %CaJSR
    %Y(33) = 0.1038669181; %CaJSR


    Y(34) = 0.45367981;  %fTC
    Y(35) = 0.93724623;  %fMC
    Y(36) = 0.05542706;  %fTMM
    Y(37) = 0.6364781;   %fCMi
    Y(38) = 0.29785784;  %fCMs
    Y(39) = 0.84628533;  %fCQ
end
%% Integration method

    [t,Yc] = ode15s(@Clara2020,[0 200000], Y , options, mflag);
    Vm   = Yc(:,1);
    dVm  = [0; diff(Vm)./diff(t)];


%%
for i= 1:size(Yc,1)
[~, dati]    = Clara2020(t(i), Yc(i,:),mflag);
    INa(i)   = dati(1);
    INas(i)  = dati(2);
    ICaL(i)  = dati(3);
    ICaD(i)  = dati(4);
    ICaT(i)  = dati(5);
    Ikr(i)   = dati(6);
    Ik1(i)   = dati(7);
    Ito(i)   = dati(8);
    Isus(i)  = dati(9);
    If(i)    = dati(10);
    IbNa(i)  = dati(11);
    IbK(i)   = dati(12);
    IbCa(i)  = dati(13);
    Ip(i)    = dati(14);
    INaCa(i) = dati(15);
    Ist(i)   = dati(16);
    IKs(i)   = dati(17);
    h1(i)    = dati (18);
    h2(i)    = dati (19);
    m(i)     = dati (20);
    d_D(i)   = dati (21);
    f_D(i)   = dati (22);
    d_T(i)   = dati (23);
    f_T(i)   = dati (24);
    Istim(i) = dati (25);
    d_s(i)   = dati (26);
    f_s(i)   = dati (27);
```

```
%gates INas
m_inf(i)  = dati(28);
tau_m(i)  = dati(29);
h1_inf(i) = dati(30);
tau_h1(i) = dati(31);
tau_h2(i) = dati(32);

%Gates of ICaD
d_D_inf (i) = dati (33);
f_D_inf (i) = dati (34);
tau_d_D (i) = dati (35);
tau_f_D (i) = dati (36);

%Gates of ICaT
d_T_inf (i) = dati (37);
f_T_inf (i) = dati (38);
tau_d_T (i) = dati (39);
tau_f_T (i) = dati (40);

%INas
ms (i)  = dati (41);
hs1 (i) = dati (42);
hs2 (i) = dati (43);

%ISK
ISK (i)   = dati(44);
m_cak (i) = dati(45);

%Ca flux
j_Ca_dif (i) = dati(46);
j_up (i)     = dati(47);
j_tr (i)     = dati(48);
j_SRCarel (i)= dati(49);

%IKACh
IKACh (i) = dati(50);

%intracellular currents
Cai(i) = dati(51);
Nai(i) = dati(52);
Ki(i)  = dati(53);

%calcium currents
Ca_sub(i) = dati(54);
CaNSR(i)  = dati(55);
CaJSR(i)  = dati(56);

 end
result       = [INa;INas; ICaL; ICaD; ICaT; Ikr; Ik1; Ito ; Isus; If; IbNa; IbK; IbCa; Ip; INaCa; Ist; IKs; h1;
h2;m; d_D; f_D; d_T;f_T; Istim; d_s; f_s; m_inf; tau_m ; h1_inf; tau_h1; tau_h2; d_D_inf; f_D_inf; tau_d_D;
tau_f_D; d_T_inf; f_T_inf; tau_d_T; tau_f_T; ms; hs1; hs2; ISK; m_cak; j_Ca_dif; j_up; j_tr; j_SRCarel; IKACh];
mat_correnti = [INa;INas; ICaL; ICaD; ICaT; Ikr; Ik1; Ito; Isus; If; IbNa; IbK; IbCa; Ip; INaCa; Ist; IKs; Istim;
ISK; IKACh];
I_tot = sum(mat_correnti);

%% Biomarkers calculation

[APA, MDP, TOP, CL, RATE, dV_dt_max, APD20, APD50, APD90, OS, DDR, DDR100, Cai_range, TA, dCai_dt_max, TD20, TD50,
TD90] = parameters(t, Vm, I_tot)
```

The code corresponding to the function *model* is th following:

```
function [dY, dati] = Clara2020(time, Y, mflag)

%SAN and AVN model

%% Constants

F  = 96485000000000000; % femtocoulomb_per_millimole
F1 = F*(10^-12);
R  = 8314400000000000; % attojoule_per_millimole_kelvin
R2 = R*(10^-12);

if mflag==1 %SAN
    T = 310.15; % K
else %AVN
    T = 310; % K
end

V  = Y(1); %mV

% time (millisecond)
% current in pA/pF
% concentration in mM

%% Cell dimension

if mflag == 1 %SAN
    Cm    = 21;       %pF
    Rcell = 0.000035; %dm
    Lcell = 0.0007;   %dm
else %AVN
    Cm      =  22;     %pF
    Rcell   = 0.00005; %dm
    Cm_surf = 1;       %uF/cm^2

    Lcell = (1/(2*pi*Rcell))*(Cm/(10^8*Cm_surf)-(2*pi*(Rcell)^2)); %dm
end

ds = 0.001; %dimensionless
%ds=0.0119093;

%litre
V_Cell = 3.1416*Rcell^2*Lcell;
V_sub  = ds*V_Cell;
V_i    = 0.46*V_Cell-V_sub;
V_JSR  = 0.0012*V_Cell;
V_NSR  = 0.0116*V_Cell;

%% Ionic concentrations (mM)
% Extracellular concentrations
Nao = 140;
Ko  = 5.4;
```

```
Cao = 2;

% Intracellular concentrations
Nai = Y(28);
Ki  = Y(29);
Cai = Y(30);

Ca_sub = Y(31);
CaJSR  = Y(33);
CaNSR  = Y(32);
%% Nernst potential (mV)

E_Na  = (R*T)/F*log(Nao/Nai);
E_Ca  = 0.5*(R*T)/F*log(Cao/Cai);
E_K   = (R*T)/F*log(Ko/Ki);
PkNa  = 0.12;
E_K_s = (R*T)/F*log((Ko+PkNa*Nao)/(Ki+PkNa*Nai));



%% INar

m  = Y(2);
h1 = Y(3);
h2 = Y(4);

if mflag==1 %SAN
    g_Na    = 3;      %nS/pF
    INa_act = -43;    %mV
    INa_In  = -65.1; %mV
    sNa     = 7;

    m_inf    = (1/(1+exp((-1)*(V-(INa_act))/(sNa))));%^(1/3);
    tau_m    = (6.247E-1)/(0.8322166*exp((-1)*(0.33566)*(V+(56.7062)))+0.6274*exp((0.0823)*(V+(65.0131))))+(4.569e-
2);
    dY(2, 1) = (m_inf-m)/tau_m;

    h1_inf   = (1/(1+exp((V-(INa_In))/(3))));
    tau_h1   = ((3.717E-3)*exp((-1)*(.2815)*(V+(17.11)))/(1+.003732*exp((-1)*(.3426)*(V+(37.76))))+(5.977E-1));
    dY(3, 1) = (h1_inf-h1)/tau_h1;

    h2_inf   = h1_inf;
    tau_h2   = ((3.186E-5)*exp((-1)*(.6219)*(V+(18.8)))/(1+7.189E-5*exp((-1)*(.6683)*(V+(34.07 ))))+(3.556));
    dY(4, 1) = (h2_inf-h2)/tau_h2;

    FNa      = .0952*exp((-1)*(.063)*(V+(34.4)))/(1+1.66*exp((-1)*(.225)*(V+(43.7))))+.0869;
    h        = ((1-FNa)*h1+FNa*h2);

    i_Na = g_Na*m^3*h*(V-E_Na); %pA/pF

else %AVN
    g_Na    = 1.1e-5/Cm*1000; %nS/pF
    INa_act = 43;             %mV
    INa_In  = 65.1;           %mV
    sNa     = 7;

    m_inf=(1/(1+exp((V+INa_act)/(-sNa))))^1/3;

    tau_m   = ((0.6247/(0.832*exp(-0.335*(V+56.7))+0.627*exp(0.082*(V+65.01))))+0.04); %ms
```

```
    dY(2, 1)= (m_inf-m)/tau_m;

    h1_inf   = 1/(1+exp((V+INa_In)/6));
    tau_h1   = (((3.717e-03*exp(-0.2815*(V+17.11)))/(1+0.003732*exp(-0.3426*(V+ 37.76))))+0.59779); %ms
    dY(3, 1) = (h1_inf-h1)/tau_h1;

    h2_inf   = h1_inf;
    tau_h2   = (((0.00003186*exp(-0.6219*(V+18.8)))/(1+0.00007189*exp(-0.6683*(V+34.07))))+3.556); %ms
    dY(4, 1) = (h2_inf-h2)/tau_h2;

    FNa = (9.52e-02*exp(-6.3e-2*(V+34.4))/(1+1.66*exp(-0.225*(V+63.7))))+8.69e-2;
    h   = (1-FNa)*h1+FNa*h2;

    i_Na = g_Na*m^3*h*Nao*(F1^2/(R2*T))*((exp((V-E_Na)*F1/(R2*T))-1)/(exp(V*F1/(R2*T))-1))*V; %pA/pF

end

%% INas

ms  = Y(5);
hs1 = Y(6);
hs2 = Y(7);

if mflag==1 %SAN
    g_Nas   = 4;    %nS/pF
    INas_ac = -31;  %mV
    INas_In = -56;  %mV
    sNas    = 4.4;

    ms_inf  = (1/(1+exp((-1)*(V-(INas_ac))/(sNas))));%^1/3;
    tau_ms  = (6.247E-1)/(.8322166*exp((-1)*(.33566)*(V+(56.7062)))+.6274*exp((.0823)*(V+(65.0131))))+(4.569E-2);
%ms
    dY(5,1) = (ms_inf-ms)/tau_ms;

    hs1_inf = (1/(1+exp((V-(INas_In))/(3))));
    tau_hs1 = ((3.717E-3)*exp((-1)*(.2815)*(V+(17.11)))/(1+.003732*exp((-1)*(.3426)*(V+(37.76))))+(5.977E-1)); %ms
    dY(6,1) = (hs1_inf-hs1)/tau_hs1;

    hs2_inf = hs1_inf;
    tau_hs2 = ((3.186E-5)*exp((-1)*(.6219)*(V+(18.8)))/(1+7.189E-5*exp((-1)*(.6683)*(V+(34.07))))+(3.556)); %ms
    dY(7,1) = (hs2_inf-hs2)/tau_hs2;

    FNas    = 0.0952*exp((-1)*(.063)*(V+(34.4)))/(1+1.66*exp((-1)*(.225)*(V+(43.7))))+.0869;
    hs      = ((1-FNas)*hs1+FNas*hs2);

    i_Nas = g_Nas*ms^3*hs*(V-E_Na); %pA/pF
else %AVN
    g_Nas   = (2.5e-06/Cm*1000)*0.066; %nS/pF reform
    INas_ac = 36; %mV reform
    INas_In = 56; %mV
    sNas    = 4; %reform

    ms_inf  = (1.0/(1+exp((V+INas_ac)/(-sNas))));%^1/3;

    tau_ms  = ((0.6247/(0.832*exp(-0.335*(V+56.7))+0.627*exp(0.082*(V+65.01))))+0.04); %ms
    dY(5,1) = (ms_inf-ms)/tau_ms;

    hs1_inf = 1/(1+exp((V+INas_In)/3));
    tau_hs1 = (((3.717e-03*exp(-0.2815*(V+17.11)))/(1+0.003732*exp(-0.3426*(V+ 37.76))))+0.5977); %ms
```

```
    dY(6,1) = (hs1_inf-hs1)/tau_hs1;

    hs2_inf = hs1_inf;
    tau_hs2 = (((0.00003186*exp(-0.6219*(V+18.8)))/(1+0.00007189*exp(-0.6683*(V+34.07))))+3.556); %ms
    dY(7,1) = (hs2_inf-hs2)/tau_hs2;

    FsNa    = (9.52e-02*exp(-6.3e-2*(V+34.4))/(1+1.66*exp(-0.225*(V+63.7))))+8.69e-2;
    hs      = (1-FsNa)*hs1+FsNa*hs2;

    i_Nas = g_Nas*ms^3*hs*Nao*(F1^2/(R2*T))*((exp((V-E_Na)*F1/(R2*T))-1)/(exp(V*F1/(R2*T))-1))*V; %pA/pF

end

%% ICaL

d_L = Y(9);
f_L = Y(10);

if mflag==1 %SAN
    fCa = Y(40);

    g_Ca_L     = 0.56;  %nS/pF
    E_Ca_L     = 45;    %mV
    ICaL_act   = -9;    %mV
    ICaL_inact = -30;   %mV

    d_L_inf   = (1/(1+exp(((-1)*(V-(ICaL_act)))/(6))));
    alpha_d_L = (((((-1)*(0.02839))*(V+(35)))/(exp(((-1)*(V+(35)))/(2.5))-1))-(((0.0849)*V)/(exp(((-1)*V)/(4.808
))-1))); %1/ms
    beta_d_L  = (((0.01143)*(V-(5)))/(exp((V-(5))/(2.5))-1)); %1/ms
    tau_d_L   = (1/(alpha_d_L+beta_d_L)); %ms
    dY(9,1)   = (d_L_inf-d_L)/tau_d_L;

    f_L_inf   = (1/(1+exp((V-(ICaL_inact))/(5))));
    tau_f_L   = ((44.3)+((257.1)*exp((-1)*(((V+(32.5))/(13.9))^2)))); %ms
    dY(10,1)  = (f_L_inf-f_L)/tau_f_L;

    Km_fCa   = 0.00035; %mM
    beta_fCa = 60;    %1/ms

    alpha_fCa    = (Km_fCa*beta_fCa); %1/ms
    fCa_infinity = (Km_fCa/(Km_fCa+Ca_sub));
    tau_fCa      = (fCa_infinity/alpha_fCa); %ms
    dY(40,1)     = ((fCa_infinity-fCa)/tau_fCa);

    i_Ca_L = g_Ca_L*(V-E_Ca_L)*d_L*f_L*fCa; %pA/pF
else %AVN
    g_Ca_L =0;
    E_Ca_L = 46.4;

    alpha_d_L = (-0.01419*((V+35.0)/(exp(-(V+35)/2.5)-1))-0.04245*V/(exp(-0.208*V)-1)); %1/ms
    beta_d_L  = (0.00571*(V-5)/(exp(0.4*(V-5))-1));  %1/ms
    tau_d_L   = 1/(alpha_d_L+beta_d_L); %ms
    d_L_inf   = 1/(1+exp(-(V+3)/5));
    dY(9,1)   = (d_L_inf-d_L)/tau_d_L;

    alpha_f_L = (0.00312*(V+28)/(exp((V+28)/4)-1)); %1/ms
    beta_f_L  = (0.025/(1+exp(-(V+28)/4))); %1/ms
    tau_f_L   = 1/(alpha_f_L+beta_f_L); %ms
```

```
    f_L_inf   = 1/(1+exp((V+36)/4.6));
    dY(10,1)  = (f_L_inf-f_L)/tau_f_L;

    i_Ca_L = g_Ca_L*(f_L*d_L+(0.006/(1+exp(-(V+14.1)/6))))*(V-E_Ca_L); %pA/pF
end
%% ICaD

d_D = Y(11);
f_D = Y(12);

if mflag==1 %SAN
    g_Ca_D    = 0.65; %nS/pF
    E_Ca_D    = 46.4; %mV
    Cav1_3act = -25;  %mV
    Cav1_3In  = -46;  %mV
    p_act     = 6.4;
    p_inact   = 4;

    v_alphamax_1 = 0.01984;
    s_alpha      = -48.8155;
    p_alpha_D_1  = 0.04481;
    v_alphamax_2 = 0.02388;
    p_alpha_D_2  = 7.47267;

    v_betamax    = 0.01049;
    s_beta_d     = 127.70831;
    p_beta_D     = 1.01728;

    d_D_inf   = 1/(1+exp((-1)*(V-Cav1_3act)/p_act));
    alpha_d_D = (((-1)*v_alphamax_1*(V+s_alpha))/(exp(-(V+s_alpha)/p_alpha_D_1)-1))-(v_alphamax_2*V/(exp(-
V/p_alpha_D_2)-1));
    beta_d_D  = v_betamax*(V-s_beta_d)/(exp((V-s_beta_d)/p_beta_D)-1);
    tau_d_D   = 1/(alpha_d_D+beta_d_D);
    dY(11,1)  = (d_D_inf-d_D)/tau_d_D;

    alpha_f_max = 0.0001068; %1/mV
    s_ab        = 26.3;      %mV
    p_ab        = 30;        %mV
    tau_f_max   = 500;       %ms
    s_tau_f     = -80;       %mV
    p_tau_f     = 12;        %mV
    tau_f_c     = 60;        %ms

    f_D_inf   = 1/(1+exp((V-Cav1_3In)/p_inact));
    alpha_f_D = alpha_f_max*exp((V+s_ab)/p_ab);  %1/ms
    beta_f_D  = alpha_f_max*exp(-(V+s_ab)/p_ab); %1/ms
    tau_f_D   = (tau_f_max*exp(-((V+s_tau_f)/p_tau_f)^2)+tau_f_c); %ms
    dY(12,1)  = (f_D_inf-f_D)/tau_f_D;

    f_F_on = 1;

        start = 3.019;%dimensionless
        kap   = 0.01698;%dimensionless
        if V<-40
            Pv = 0;
        else
            Pv = start*exp(kap*V);%dimensionless
        end

        bot   = -18.8;%dimensionless
```

```
        slope = 163.5;%dimensionless
        top   = 23.21;%dimensionless
        vc    = 35.72;%dimensionless

        if time==0
            val = 0;
        else
            val = 1;
        end

    Pi = (val*(bot+((top-bot)/(1+(exp((vc-time)/slope))))));

        f_F = (1+f_F_on*(Pv+Pi)/100);

    i_Ca_D = g_Ca_D*(V-E_Ca_D)*d_D*f_D*fCa*f_F; %pA/pF

else %AVN
    g_Ca_D = (0.004/Cm*1000)*0.345; %nS/pF
    E_Ca_D = 34.5; %mV

    Cav1_3act = 22;
    Cav1_3In  = 48;

    alpha_d_D = (-0.01419*((V+35.0)/(exp(-(V+35)/2.5)-1))-0.04245*V/(exp(-0.208*V)-1)); %1/ms
    beta_d_D  = (0.00571*(V-5)/(exp(0.4*(V-5))-1));                                     %1/ms
    tau_d_D   = 1/(alpha_d_D+beta_d_D);                                                 %ms
    d_D_inf   = 1/(1+exp(-(V+Cav1_3act)/6.3));
    dY(11,1)  = (d_D_inf-d_D)/tau_d_D;

    alpha_f_D = (0.00312*(V+28)/(exp((V+28)/4)-1)); %1/ms
    beta_f_D  = (0.025/(1+exp(-(V+28)/4)));         %1/ms
    tau_f_D   = 1/(alpha_f_D+beta_f_D);             %ms
    f_D_inf   = 1/(1+exp((V+Cav1_3In)/5.4));
    dY(12,1)  = (f_D_inf-f_D)/tau_f_D;

    i_Ca_D = g_Ca_D*(f_D*d_D+(0.006/(1+exp(-(V+14.1)/6))))*(V-E_Ca_D); %pA/pF
end

%% ICaT
d_T = Y(13);
f_T = Y(14);

if mflag==1 %SAN
    g_Ca_T = 0.32;
    E_Ca_T = 45;

    d_T_inf  = (1/(1+exp(((-1)*(V+(26.3)))/(6))));
    tau_d_T  = ((1)/(((1.068)*exp((V+(26.3))/(30)))+((1.068)*exp(((-1)*(V+(26.3))))/(30))))); %ms
    dY(13,1) = (d_T_inf-d_T)/tau_d_T;

    f_T_inf  = (1/(1+exp((V+(61.7))/(5.6))));
    tau_f_T  = ((1)/(((0.0153)*exp(((-1)*(V+(61.7))))/(83.3)))+((0.015)*exp((V+(61.7))/(15.38))))); %ms
    dY(14,1) = (f_T_inf-f_T)/tau_f_T;
else %AVN
    g_Ca_T   = (0.0068/Cm*1000)*0.83; %nS/pF
    Cav3_1ac = 39;                    %mV

    E_Ca_T   = E_Ca_D; %mV
    Cav3_1In = 71;     %mV
```

```
    alpha_d_T = 1.068*exp((V+26.3)/30);  %1/ms
    beta_d_T  = 1.068*exp(-(V+26.3)/30); %1/ms
    tau_d_T   = 1/(alpha_d_T+beta_d_T);  %ms
    d_T_inf   = 1/(1+exp(-(V+Cav3_1ac)/4.64));
    dY(13,1)  = (d_T_inf-d_T)/tau_d_T;

    alpha_f_T = 0.0153*exp(-(V+71.7)/83.3); %1/ms
    beta_f_T  = 0.015*exp((V+71.7)/15.38);  %1/ms
    tau_f_T   = 1/(alpha_f_T+beta_f_T);     %ms
    f_T_inf   = 1/(1+exp((V+Cav3_1In)/3.4));
    dY(14,1)  = (f_T_inf-f_T)/tau_f_T;

end

i_Ca_T = g_Ca_T*d_T*f_T*(V-E_Ca_T); %pA/pF

%%  IK1
if mflag==1 %SAN
    gk1  = 0; %nS/pF

    i_K1 = gk1*(V-E_K); %pA/pF
else %AVN
    gk1  = 0.001525/Cm*1000; %nS/pF

    i_K1 = gk1*(V-E_K)/(1+exp(0.07*(V+80.0))); %pA/pF
end

%% IKr
F_K_r = 0.4;

P_af =  Y(15);
P_as =  Y(16);
P_i  =  Y(17);
P_a  =  (1-F_K_r)*P_af+F_K_r*P_as;

if mflag==1 %SAN
    g_K_r = 0.15;

    P_af_inf = (1/(1+exp(((-1)*(V+(23.2)))/(10.6))));
    tau_P_af = ((0.84655354)/(((0.0372)*exp(V/(15.9)))+((0.00096)*exp(((-1)*V)/(22.5))))); %ms
    dY(15,1) = (P_af_inf-P_af)/tau_P_af;

    P_as_inf = P_af_inf;
    tau_P_as = ((0.84655354)/(((0.0042)*exp(V/(17)))+((0.00015)*exp(((-1)*V)/(21.6))))); %ms
    dY(16,1) = (P_as_inf-P_as)/tau_P_as;

    P_i_inf  = (1/(1+exp((V+(28.6))/(17.1))));
    tau_P_i  = ((1)/(((0.1)*exp(((-1)*V)/(54.645)))+((0.656)*exp(V/(106.157))))); %ms
    dY(17,1) = (P_i_inf-P_i)/tau_P_i;

else %AVN
    g_K_r = 0.005/Cm*1000; %nS/pF

    Pinac = -15;

    P_af_inf = 1/(1+exp(-(V+23)/6.5));
    tau_P_af = (0.84655/(0.0372*exp(V/15.9)+0.00096*exp(-V/22.5))); %ms
    dY(15,1) = (P_af_inf-P_af)/tau_P_af;
```

```
    P_as_inf = P_af_inf;
    tau_P_as = (0.84655/(0.0042*exp(V/17)+0.00015*exp(-V/21.6)));  %ms
    dY(16,1) = (P_as_inf-P_as)/tau_P_as;

    tau_P_i  = 2;  %ms
    P_i_inf  = 1/(1+exp((V+(-Pinac))/6.5));
    dY(17,1) =(P_i_inf-P_i)/tau_P_i;
end

i_K_r = g_K_r*P_a*P_i*(V-E_K); %pA/pF


%% Ito and Isus

q = Y(18);
r = Y(19);

if mflag==1 %SAN
    g_to  = 0; %nS/pF
    g_sus = 0; %nS/pF

    q_inf    = (1/(1+exp((V+(49))/(13))));
    tau_q    = (((65.17)/((0.57*exp(((-1)*0.08)*(V+(44))))+(0.065*exp(0.1*(V+(45.93)))))))+(10.1)); %ms
    dY(18,1) = (q_inf-q)/tau_q;

    r_inf    = (1/(1+exp(((-1)*(V-(19.3)))/(15))));
    tau_r    = (((24.826)/((1.037*exp(0.09*(V+(30.61))))+(0.369*exp(((-1)*0.12)*(V+(23.84)))))))+(4.172)); %ms
    dY(19,1) = (r_inf-r)/tau_r;
else %AVN
    g_to  = (0.000491/Cm*1000)*2.74; %nS/pF

    g_sus = 0.0000665/Cm*1000;       %nS/pF

    q_inf    = 1/(1+exp((V+59.37)/13.1));
    tau_q    = (10.1+(65.17/(0.57*exp(-0.08*(V+49)))+0.000024*exp(0.1*(V+50.93))));    %ms
    dY(18,1) = (q_inf-q)/tau_q;

    r_inf    = 1/(1+exp(-(V-10.93)/19.7));
    tau_r    = (2.98+(15.59/(1.037*exp(0.09*(V+30.61))+0.369*exp(-0.12*(V+23.84))))); %ms
    dY(19,1) = (r_inf-r)/tau_r;
end

i_to  = g_to*q*r*(V-E_K); %pA/pF
i_sus = g_sus*r*(V-E_K);  %pA/Pf

%% Iks

xs = Y(23);

if mflag==1 %SAN
    g_K_s = 0; %nS/pF
else %AVN
   g_K_s  = 0.000518/Cm*1000; %nS/pF
end

alpha_xs = (0.014/(1+exp(((-1)*(V-40))/9))); %1/ms
```

```
beta_xs  = (0.001*exp(((-1)*V)/45));          %1/ms
xs_inf   = (alpha_xs/(alpha_xs+beta_xs));
tau_xs   = (1/(alpha_xs+beta_xs));            %ms
dY(23,1) = (xs_inf-xs)/tau_xs;

i_K_s = g_K_s*xs^2*(V-E_K_s); %pA/pF

%% If

if_flag = 1; % if block flag

P = Y(20);

%cAMP
vslope = 6.3;
naff   = 0.782;
Vr     = 15.02; %mV

K_R = 0.0000578; %mM
K_T = 0.0005416; %mM

if mflag==1 %SAN
    g_f    = 0.5;     %nS/pF
    g_f_Na = g_f*0.5; %nS/pF
    g_f_K  = g_f*0.5; %nS/pF

    alp0 = 0.283;
    bet0 = 83000.1;
    cAMP = 0.000025; %mM

    Vf     = -90; %mV
    s_If   = 14;
    If_act = -80;

    scAMP = vslope*naff*log((1+cAMP/K_R)/(1+cAMP/K_T));

    P_inf    = 1/(1+exp((V-Vf-scAMP)/s_If));
    alpha_P  = 0.0000196*exp(-(V/19.58724)); %1/ms
    beta_P   = 0.1326129*exp(V/19.58724);    %1/ms
    tau_P    = 1/(alpha_P+beta_P);           %ms
    dY(20,1) = (P_inf-P)/tau_P;

    i_f_Na = g_f_Na*P^2*(V-E_Na); %pA/pF
    i_f_K  = g_f_K*P^2*(V-E_K);   %pA/pF

else %AVN
    gh = 0.228*25;
    gh = (gh/Cm)*0.8; %nS/pF

    P_inf    = 1/(1+exp((V+97)/20));
    tau_P    = 1.505./(exp(-0.0119*(V+590.3))+exp((V-55)/17.2)); %ms
    dY(20,1) = (P_inf-P)/tau_P;

    i_f_Na = 0.3833*gh*P*(V-E_K);  %pA/pF
    i_f_K  = 0.3833*gh*P*(V-E_Na); %pA/pF

end
```

```
i_f = (i_f_Na+i_f_K)*if_flag; %pA/pF



%% sodium_background_current

if mflag==1 %SAN
    g_b_Na = 0.002; %nS/pF
else %AVN
    g_b_Na = 0.000058/Cm*1000; %nS/pF
end

i_b_Na = g_b_Na*(V-E_Na); %pA/pF

%% potassium_background_current

if mflag==1 %SAN
    g_b_K = 0.0054; %nS/pF
else %AVN
    g_b_K = 0.0000252/Cm*1000; %nS/pF
end

i_b_K = g_b_K*(V-E_K); %pA/pF

%% calcium_background_current
if mflag==1 %SAN
    g_b_Ca = 0.0005; %nS/pF
else %AVN
    g_b_Ca = 0.0000132/Cm*1000; %nS/pF
end

i_b_Ca = g_b_Ca*(V-E_Ca); %pA/pF

%% sodium_potassium_pump

if mflag==1 %SAN
    K_m_Na = 14;  %mM
    K_m_K  = 1.4; %mM

    i_p_max = 3.6; %pA

    i_p = (((i_p_max*((1+((K_m_K/Ko)^1.2))^((-1)*1)))*((1+((K_m_Na/Nai)^1.3))^((-1)*1)))*((1+exp(((-1)*((V-
E_Na)+(120)))/(30)))^((-1)*1))); %pA/pF
else %AVN
    K_m_Na = 5.64;  %mM
    K_m_K  = 0.621; %mM

    i_p_max = 47.8; %pA

    i_p = (i_p_max*(Nai/(K_m_Na+Nai))^3*(Ko/(K_m_K+Ko))^2*1.6/(1.5+exp(-(V+60)/40)))/Cm; %pA/pF

end

%% sodium calcium exchanger I NaCa
if mflag==1 %SAN
    kNaCa = 125;

    %mM
```

```
    Kci = 0.0207;
    Kcni = 26.44;
    K1ni = 395.3;
    K2ni = 2.289;
    K3ni = 26.44;
    K1no = 1628;
    K2no = 561.4;
    K3no = 4.663;
    Kco  = 3.663;

    %dimensionless
    Qci = 0.1369;
    Qn  = 0.4315;
    Qco = 0;

    %dimensionless
        di=((1+((Ca_sub/Kci)*((1+exp(((((-
1)*Qci)*V)*F)/(R*T)))+(Nai/Kcni))))+((Nai/K1ni)*(1+((Nai/K2ni)*(1+(Nai/K3ni))))));
        do=((1+((Cao/Kco)*(1+exp(((Qco*V)*F)/(R*T)))))+(((Nao/K1no)*(1+(Nao/K2no)))*(1+(Nao/K3no))));

        k12=(((Ca_sub/Kci)*exp(((((-1)*Qci)*V)*F)/(R*T)))/di);
        k21=(((Cao/Kco)*exp(((Qco*V)*F)/(R*T)))/do);
        k43=(Nai/(K3ni+Nai));
        k14=((((((Nai/K1ni)*Nai)/K2ni)*(1+(Nai/K3ni)))*exp(((Qn*V)*F)/((2*R)*T)))/di);
        k41=exp(((((-1)*Qn)*V)*F)/((2*R)*T));
        k34=(Nao/(K3no+Nao));
        k23=((((((Nao/K1no)*Nao)/K2no)*(1+(Nao/K3no)))*exp(((((-1)*Qn)*V)*F)/((2*R)*T)))/do);
        k32=exp(((Qn*V)*F)/((2*R)*T));

        x1=(((k41*k34)*(k23+k21))+((k21*k32)*(k43+k41)));
        x2=(((k32*k43)*(k14+k12))+((k41*k12)*(k34+k32)));
        x3=(((k14*k43)*(k23+k21))+((k12*k23)*(k43+k41)));
        x4=(((k23*k34)*(k14+k12))+((k14*k21)*(k34+k32)));

     i_NaCa = ((kNaCa*((x2*k21)-(x1*k12)))/(((x1+x2)+x3)+x4)); %pA/pF
else %AVN
    iNaCa_flag = 0.5;
    K_NaCa     = 0.00005*iNaCa_flag;
    d_NaCa     = 0.0001;
    gammaNaCa  = 0.5;

    i_NaCa = (1000/10*K_NaCa*((Nai^3*Cao*exp(0.03743*V*gammaNaCa)-Nao^3*Cai*exp(0.0374*V*(gammaNaCa-
1)))/(1+d_NaCa*(Cai*Nao^3+Cao*Nai^3))))/Cm; %pA/pF
end



%%  Ist
d_s = Y(21);
f_s = Y(22);

E_st = 10;

if mflag==1 %SAN
    g_st = 0.01; %nS/pF

    d_s_inf   = (1/(1+exp(((-1)*(V+57))/5)));
    alpha_d_s = (1/(((0.15)*exp(((-1)*V)/(11)))+((0.2)*exp(((-1)*V)/(700))))); %1/ms
    beta_d_s  = (1/(((16)*exp(V/(8)))+((15)*exp(V/(50))))); %1/ms
    tau_d_s   = (1/(alpha_d_s+beta_d_s)); %ms
    dY(21,1)  = (d_s_inf-d_s)/tau_d_s;
```

```
    alpha_f_s = (1/((3100*exp(V/13))+(700*exp(V/70))));                                          %1/ms
    beta_f_s  = ((1/((95*exp(((-1)*V)/10))+(50*exp(((-1)*V)/700))))+(2.29E-4/(1+exp(((-1)*V)/5)))); %1/ms
    tau_f_s   = (6.65/(alpha_f_s+beta_f_s));                                                      %ms
    f_s_inf   = alpha_f_s/(alpha_f_s+beta_f_s);
    dY(22,1)  = (f_s_inf-f_s)/tau_f_s;

else %AVN
    g_st = 0.017/Cm*1000; %nS/pF

    alpha_d_s = 1/(0.15*exp(-V/11)+0.2*exp(-V/700)); %1/ms
    beta_d_s  = 1/(16*exp(V/8)+15*exp(V/50));        %1/ms
    tau_d_s   = 1/(alpha_d_s+beta_d_s);              %ms
    d_s_inf   = alpha_d_s/(alpha_d_s+beta_d_s);
    dY(21,1)  = (d_s_inf-d_s)/tau_d_s;

    alpha_f_s = 1/(3100*exp(-V/13)+700*exp(-V/70));                    %1/ms
    beta_f_s  = 1/(95*exp(-V/10)+50*exp(V/700))+2.29e-4/(1+exp(-V/5)); %1/ms
    tau_f_s   = 1/(alpha_f_s+beta_f_s);                                %ms
    f_s_inf   = alpha_f_s/(alpha_f_s+beta_f_s);
    dY(22,1)  = (f_s_inf-f_s)/tau_f_s;
end

i_st = g_st*d_s*f_s*(V-E_st); %pA/pF

%% calcium_dependent_potassium_channel
g_SK  = 0.004; %nS/pF

m_cak = Y(24);

beta_k = 100;
n_SK   = 1.7;
Cac    = 0.000007; %mM

Car=((Ca_sub/Cac)^n_SK); %mM

m_inf_cak = Car/(1+Car);
tau_cak   = (10^(-3))/( beta_k*(1+Car)); %ms
dY(24,1)  = (m_inf_cak-m_cak)/tau_cak;

i_SK = g_SK*m_cak^2*(V-E_K); %pA/pF

%% background_muscarinic_potassium_channel_current
%g_K_ACh=((0.0000)*(Ko^0.41));
g_K_ACh =((0.0010)*(Ko^0.41)); %nS/pF

i_K_ACh = (g_K_ACh*(Ki-(Ko*exp((((-1)*V)*F)/(R*T))))); %pA/pF

%% intracellular_calcium_dynamics

R1 = Y(25);
O1 = Y(26);
I1 = Y(27);
RI =(1-R1-O1-I1);

tau_dif_Ca = 0.04; %1/ms
tau_tr     = 60;   %1/ms
```

```
if mflag==1 %SAN
    ks   = 250;   %1/ms
    P_up = 0.005; %mM/ms
    K_up = 0.006; %mM
else %AVN
    ks   = 250;  %1/ms
    P_up=0.005;  %mM/ms
    K_up=0.0006; %mM
end

Ca_SR = (CaJSR-Ca_sub);

j_up      = (P_up/(1+(K_up/Cai)));  %mM/ms
j_tr      = ((CaNSR-CaJSR)/tau_tr); %mM/ms
j_SRCarel = ks*O1*(CaJSR-Ca_sub);   %mM/ms

MaxSR = 15;       %dimensionless
MinSR = 1;        %dimensionless
HSR   = 2.5;      %dimensionless
EC50_SR= 0.45;    %mM

koCa = 1.5;          %1/mM^2*ms
kom  = 0.06;         %1/ms
kiCa = 0.05;         %1/mM*ms
kim  = 0.005;        %1/mM*ms

kCaSR  = MaxSR-((MaxSR-MinSR)/(1+(EC50_SR/CaJSR)^HSR)); %dimensionless
koSRCa = (koCa/kCaSR); %1/mM^2*ms
kiSRCa = (kiCa*kCaSR); %1/mM*ms

dY(25,1) = (kim*RI-kiSRCa*Ca_sub*R1-(koSRCa*Ca_sub^2*R1-kom*O1)); %dR/dt
dY(26,1) = (koSRCa*Ca_sub^2*R1-kom*O1-(kiSRCa*Ca_sub*O1-kim*I1)); %dO/dt
dY(27,1) = (kiSRCa*Ca_sub*O1-kim*I1-(kom*I1-koSRCa*Ca_sub^2*RI)); %dI/dt

%% Ca+2 diffusion

j_Ca_dif =((Ca_sub-Cai)/tau_dif_Ca); %mM/ms

%% intracellular_ion_concentrations

ICaDout = 0.29; %dimensionless
ICaDRY  = 0.71; %dimensionless

%mM
CM_tot  = 0.045;
TC_tot  = 0.031;
TMC_tot = 0.062;
CQ_tot  = 10;

% 1/ms*mM
kf_TC  = 88.8;
kf_TMC = 227.7;
kf_TMM = 2.277;
kf_CM  = 227.7;
kf_CQ  = 0.534;

% 1/ms
kb_TC  = 0.446;
kb_TMC = 0.00751;
```

```
kb_TMM = 0.751;
kb_CM  = 0.542;
kb_CQ  = 0.445;

Mgi = 2.5; %mM

%mM
fTC  = Y(34);
fTMC = Y(35);
fTMM = Y(36);
fCMi = Y(37);
fCMs = Y(38);
fCQ  = Y(39);

%flux
delta_fTC  = (((kf_TC*Cai)*((1)-fTC))-(kb_TC*fTC));
delta_fTMC = (((kf_TMC*Cai)*((1)-(fTMC+fTMM)))-(kb_TMC*fTMC));
delta_fTMM = (((kf_TMM*Mgi)*((1)-(fTMC+fTMM)))-(kb_TMM*fTMM));
delta_fCMi = ((kf_CM*Cai)*((1)-fCMi))-(kb_CM*fCMi);
delta_fCMs = (((kf_CM*Ca_sub)*((1)-fCMs))-(kb_CM*fCMs));
delta_fCQ  = (((kf_CQ*CaNSR)*((1)-fCQ))-(kb_CQ*fCQ));

dY(28,1) = (-(i_f_Na+i_st+i_Nas+i_Na+i_b_Na+3*i_p+3*i_NaCa)*Cm)/(F*(V_i+V_sub)); %dNai/dt
dY(29,1) = (-(i_K_r+i_K_s+i_to+i_sus+i_SK+i_K1+i_f_K+i_K_ACh+(-2*i_p)+i_b_K)*Cm/(F*(V_i+V_sub))); %dKi/dt
dY(30,1) = (((((((-1)*(i_Ca_L+i_Ca_T+i_b_Ca+i_Ca_D*ICaDout)-(2*0.2*i_NaCa)))*Cm/(2*F))+(j_Ca_dif*V_sub)-
(j_up*V_NSR))/V_i)-(((CM_tot*delta_fCMi)+(TC_tot*delta_fTC))+(TMC_tot*delta_fTMC))); %dCai/dt
dY(31,1) = (((((((-1)*((ICaDRY*i_Ca_D)-(2*0.8*i_NaCa)))*Cm)/(2*F))+((j_SRCarel)*V_JSR))/V_sub)-
(j_Ca_dif+(CM_tot*delta_fCMs))); %dCa_sub/dt
dY(32,1) = (j_up-((j_tr*V_JSR)/V_NSR));%dCaNSR/dt
dY(33,1) = (j_tr-(j_SRCarel+(CQ_tot*delta_fCQ))); %dCaJSR/dt

%% calcium_buffering

dY(34,1) = delta_fTC;  %dYfTC/dt
dY(35,1) = delta_fTMC; %dYfMC/dt
dY(36,1) = delta_fTMM; %dYfTMM/dt
dY(37,1) = delta_fCMi; %dYfCMi/dt
dY(38,1) = delta_fCMs; %dYfCMs/dt
dY(39,1) = delta_fCQ;  %dYfCQ/dt


%% Stimulation
i_stim_Amplitude        = 0;   %nanoampere (in stim_mode)
i_stim_End              = 1000.0;   % second (in stim_mode)
i_stim_PulseDuration    = 0.001;   % second (in stim_mode)
i_stim_Start            = 0.0;   % second (in stim_mode)
i_stim_frequency        = 300.0;   % per_minut (in stim_mode)
stim_flag               = 1;   % dimensionless (in stim_mode)
i_stim_Period           = 60.0/i_stim_frequency;

if ((time >= i_stim_Start) && (time <= i_stim_End) && (time-i_stim_Start-floor((time-
i_stim_Start)/i_stim_Period)*i_stim_Period <= i_stim_PulseDuration))
    i_stim = stim_flag*i_stim_Amplitude/Cm;
else
    i_stim = 0.0;
end
%% Membrane potential
dY(1, 1) =( -(i_Na+i_Nas+i_Ca_L+i_Ca_D+i_Ca_T+i_K1+i_K_r+i_to+i_sus+ i_f+ i_K_s + i_b_Na+i_b_K+i_b_Ca+i_p+i_NaCa+
i_st+ i_SK+ i_K_ACh )) +i_stim;
```

```
%% Output variables
INa   = i_Na;
INas  = i_Nas;
ICaL  = i_Ca_L;
ICaD  = i_Ca_D;
ICaT  = i_Ca_T;
Ik1   = i_K1;
Ikr   = i_K_r;
Ito   = i_to;
Isus  = i_sus;
If    = i_f;
IKs   = i_K_s;
IbNa  = i_b_Na;
IbK   = i_b_K;
IbCa  = i_b_Ca;
Ip    = i_p;
INaCa = i_NaCa;
Ist   = i_st;
Istim = i_stim;
ISK   = i_SK;
IKACh = i_K_ACh;
dati  = [INa, INas, ICaL , ICaD, ICaT, Ikr,Ik1, Ito, Isus, If, IbNa, IbK, IbCa, Ip, INaCa, Ist, IKs, h1, h2,m, d_D,
f_D, d_T,f_T, Istim, d_s, f_s, m_inf, tau_m,h1_inf, tau_h1, tau_h2, d_D_inf, f_D_inf, tau_d_D,tau_f_D, d_T_inf,
f_T_inf, tau_d_T,tau_f_T, ms, hs1, hs2, ISK, m_cak , j_Ca_dif, j_up, j_tr, j_SRCarel, IKACh, Cai,Nai, Ki, Ca_sub,
CaNSR, CaJSR,O1, R1, I1, tau_P, xs];
end
```